RSC Advances

PAPER

View Article Online
View Journal | View Issue

Cite this: *RSC Adv.*, 2024, **14**, 26524

Glucospanlastics: innovative antioxidant and anticancer ascorbyl-2-glucoside vesicles for striking topical performance of repurposed itraconazole†

Caroline Lamie,[ac] Enas Elmowafy,[b] Dalia Attia *[a] and Nahed D. Mortada[b]

Presently, the development of functional derivatives exploiting biocompatible pharmaceutical materials has become a pressing demand. Among them, ascorbyl-2-glucoside (AA-2G), an ascorbic acid derivative, has significant potential owing to its stability, solubilization and antioxidant prospects. Herein, AA-2G was utilized for the fabrication of itraconazole (ITZ) spanlastics, which were denoted as "glucospanlastics". Subsequently, the newly designed glucospanlastics were characterized to determine their dimensions, charge, entrapment, solubilization efficiency, morphology, stability and antioxidant activity. Further, their cytotoxicity towards A431 cells and their *ex vivo* skin deposition were investigated. Subsequently, the competence of the formulated cream containing glucospanlastics to suppress Ehrlich carcinoma and modulate the antioxidant profile was evaluated *in vivo*. The results revealed that the proposed nano-sized glucospanlastics performed better than conventional spanlastics (without AA-2G) with respect to optimal solubilization efficiency and ITZ entrapment (>95%) together with antioxidant, cytotoxic and skin permeation potentials. More importantly, glucospanlastics containing 10 and 20 mg AA-2G demonstrated considerable tumor suppression and necrosis, improvement in glutathione (GSH) content by 1.68- and 2.26-fold, elevation of total antioxidant capacity (TAC) levels by 1.67- and 2.84-fold and 1.78- and 2.03-fold reduction in malondialdehyde (MDA) levels, respectively, compared to a conventional ITZ cream. These innovative antioxidant vesicles show future potential for the dermal delivery of cancer-directed therapies.

Received 14th May 2024
Accepted 18th July 2024

DOI: 10.1039/d4ra03542a

rsc.li/rsc-advances

1. Introduction

Currently, the pharmaceutical processing and manipulation of existing materials are increasingly evolving for the development of new modified materials possessing unique and multifunctional features, allowing for their utilization in diverse innovative delivery platforms.[1] However, in this field, there is still room for the development, commercialization and implementation of these multifunctional molecule-based products. Indeed, methodologically robust studies have been conducted by drug developers for the synthesis and elucidation of their functionality, toxicity and potency.

In this case, considering that the natural antioxidant ascorbic acid (AA) is an easy target for thermal, pH-dependent and oxidative degradation, its derivatization is necessary.[2] Thus, to address the above-mentioned issues, hydrophilic and lipophilic ascorbic acid derivatives are becoming increasingly attractive, showing superiority to ascorbic acid in terms of improved stability and antioxidant efficacy.[3] According to the literature, the application of these derivatives in various industrial sectors as solubilizing agents, stabilizing agents, antioxidants, permeation enhancers and integral components of assorted delivery vehicles have been scrutinized.[4–7]

Among the various candidates, ascorbyl glucoside (AA-2G) is a derivative of ascorbic acid with exceptional properties for application in pharmaceuticals and cosmetics (Fig. 1 and 2(A)).[8] Besides its antioxidant potential, the antitumor activity of AA-2G was verified in previous reports.[9–11] AA-2G has been patented as a skin lightening agent in skin care vehicles and an auxiliary component in an ophthalmic product containing gold nanoparticles.[12,13] Recently, AA-2G has been explored as an AA derivative prodrug in commercial formulations, showing a high

[a]*Department of Pharmaceutics and Pharmaceutical Technology, The British University in Egypt, Cairo, 11837, Egypt. E-mail: dalia.rhman@bue.edu.eg; Fax: +20-2-26300010/20; Tel: +20-2-01111414144*

[b]*Department of Pharmaceutics and Industrial Pharmacy, Faculty of Pharmacy, Ain Shams University, Monazzamet Elwehda Elafrikeya Street, Abbaseyya, Cairo, 11566, Egypt*

[c]*Drug Discovery, Delivery and Patient Care (DDDPC), School of Life Sciences, Pharmacy and Chemistry, Kingston University London, Kingston Upon Thames, Surrey, KT1 2EE, UK*

† Electronic supplementary information (ESI) available. See DOI: https://doi.org/10.1039/d4ra03542a

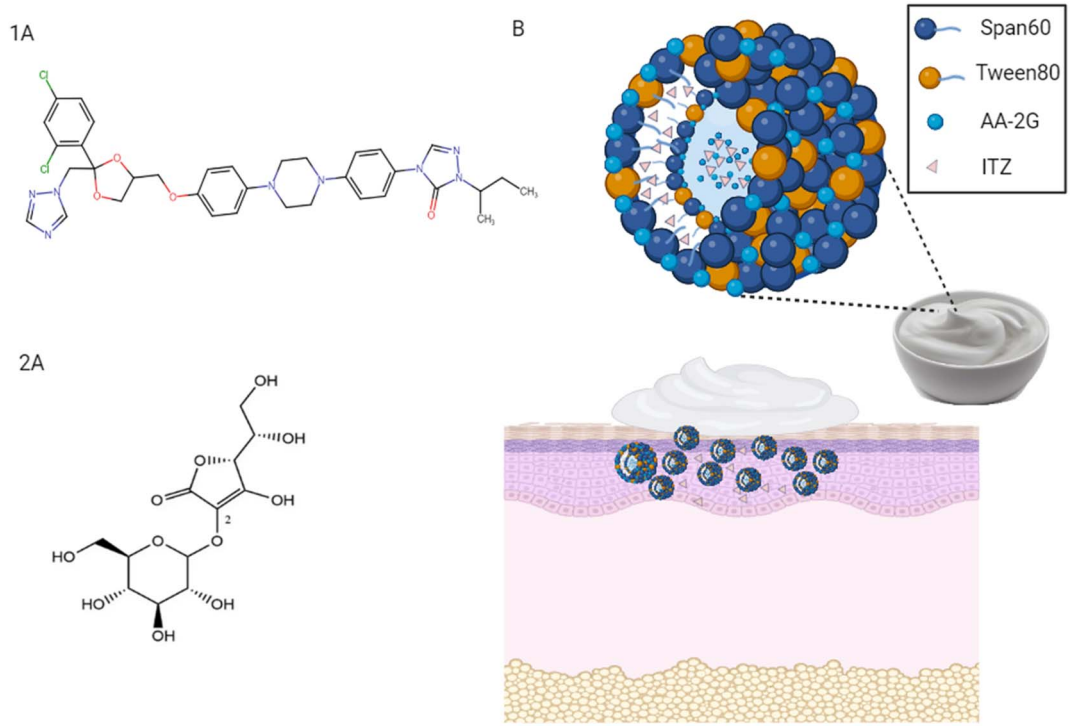

Fig. 1 Schematic representation of (1A) the chemical structure of itraconazole created by Marvin JS and (2A) chemical structure of AA-2G created using ChemDraw 16. (B) Glucospanlastics vesicle in cream base and its permeation through the skin layers.

antioxidative protective effect. Interestingly, utilizing AA-2G at a considerably low concentration of 1.8% was found to yield the same effect yielded by a high concentration (15%) of AA.[11] AA-2G is commercially available in a brightening water-based serum as an antiaging/antioxidant support (The Ordinary®, Ulta Beauty company). Following localized skin delivery, AA-2G is well-documented to be subjected to hydrolysis by α-glucosidase and transformed to L-ascorbic acid.[8]

Lately, from the perspective of drug delivery systems, AA-2G has been identified as a solubilizing agent for drugs possessing poor aqueous solubility.[4] The capability of AA-2G to enhance their solubility can be attributed to its augmented wettability and dispersibility as well as the formation of an amorphous drug form, as reported earlier.[14–16]

Recently, AA-2G has been utilized as a biologically relevant molecule and incorporated in a variety of platforms such as

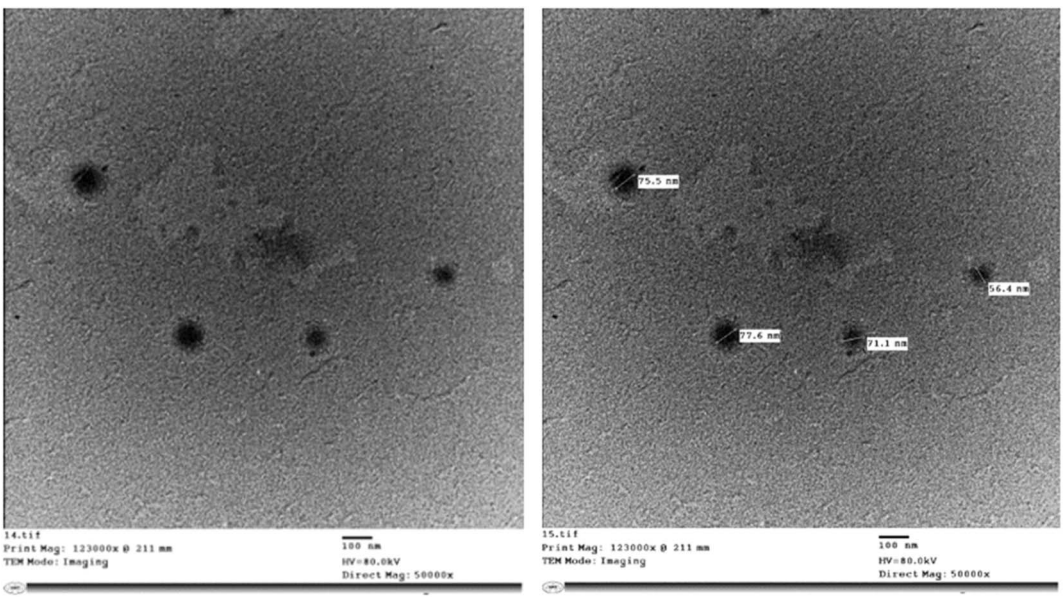

Fig. 2 TEM images of medicated glucospanlastics containing ascorbyl glucoside AA-2G as a component ($P_{CG}2$).

microneedles for transdermal delivery,[17] gels for dermal delivery,[18] and oily nanodispersions for transcorneal delivery.[19] Thus, considering the functional features and solubilizing capability of AA-2G, it is feasible that AA-2G can enhance the solubility of itraconazole (ITZ). ITZ is a weak base that possesses very low aqueous solubility (Fig. 1(1A)).[20] ITZ is an antifungal drug, which has attracted significant attention recently as an anticancer drug in various cancer types.[21] The repurposing of ITZ as an anticancer drug was first reported by Chong *et al.*[22] Specifically, ITZ was repurposed in the field of cancer treatment based on several investigations, as follows: (i) its adequate hinderance of a specific activated pathway in basal cell carcinoma, the Hedgehog pathway, by targeting smoothened protein 'SMO', (ii) its considerable prohibition of angiogenesis and tumor vascularity, accompanied by a reduction in the proliferation of endothelial cells and (iii) its induction of autophagocytosis, apoptosis and tumor necrosis, as shown in Fig. S1.†[23] Indeed, topical ITZ application specifically potentiated its local availability by maximizing its therapeutic levels with reduced drug side effects.[7]

In principle, we hypothesized that AA-2G could break new ground in designing a new platform for dermal delivery. Thus, the aim of our work was exploring the possibility of forming spanlastics using AA-2G as an integral part. Accordingly, spanlastic vesicles composed of Span 60 and Tween 80 were prepared in the presence of AA-2G (so-called glucospanlastics). Interestingly, spanlastic "sorbitan-based nanovesicles" are superior to other surfactant-based vesicular systems, which are rigid, with respect to enclosing edge activators in their structure. Edge activators are single-chain surfactants that are efficiently employed to decrease the interfacial tension between the vesicular membrane and their surrounding environment, facilitating the squeezing of the formed vesicles through small dermal pores or channels, and hence their flexibility and deformability. Accordingly, this can allow vesicles to adapt their dimensions and shape to considerably penetrate the dermal strata, fulfilling their role of conveying their enclosed cargos to the affected site (see Fig. 1(B)).[24,25]

Importantly, the heightened mobility and penetrability of the proposed spanlastic membrane can yield greater release and diffusion of the loaded drugs. Therefore, the incorporation of edge activators within the surfactant bilayer imparts higher elasticity to the vesicles, and subsequently facilitates their dermal delivery, leading to an enhancement in permeation and higher localized drug concentrations.[26,27] Additionally, the antioxidant properties of ascorbyl glucoside (AA-2G) can contribute to the functionality of the proposed glucospanlastics and their therapeutic efficacy. Optimally, the enhanced permeation of the proposed glucospanlastics could promote the retention of AA-2G in different skin strata. A recent study reported the improved permeation of AA-2G from raw clay-based O/W emulsions.[28]

Herein, in-depth characterization and stability studies were conducted. To support our hypothesis, the suitability of this system for dermal delivery was assessed by skin permeation profiling using confocal microscopy. To assess its potential impact in a therapeutic application for skin cancer, we carried out an *in vitro* antioxidant potential and cytotoxicity study on the A431 cell line employing the selected glucospanlastics. Exposure of the skin to ultraviolet radiation leads to the generation of free radicals and DNA oxidation, and hence the development of oxidative stress exceeding the endogenous defense caused by dermal antioxidants.[29] As an antioxidant, topically applied ascorbic acid can mediate the direct formation of the ascorbyl radical and H_2O_2 in the extracellular tissue near cancer cells, leading cytotoxicity.[30] Thus, to investigate the cytotoxicity of this system, A431 cells were used as model cells representing human epidermoid carcinoma cells (epithelial cells of epidermis). The utilization of A431 cells to explore the cytotoxicity of anti-cancer drugs has been reported earlier.[31,32]

Further, an *in vivo* anticancer study in rats was performed *via* the induction of Ehrlich carcinoma, with subsequent biochemical and histopathological assessments using the glucospanlastics in a cream base. The utilization of Ehrlich carcinoma cells as a model to represent skin cancer has been previously reported in the literature.[7,33]

To the best of our knowledge, the feasible contribution of AA-2G in spanlastics for the dermal delivery of the repositioned ITZ has not been investigated to date.

2. Materials and methods

2.1. Materials

Itraconazole powder was obtained from Orkila, Spansules (India). 2-*O*-Alpha-D-glucopyranosyl-L-ascorbic acid "ascorbyl glucoside", 99.5%, was sourced from INTERNATIONAL CO. for Scientific and Medical Supplies. Chloroform and ethanol (HPLC analytical grade solvents), potassium dihydrogen phosphate, disodium hydrogen phosphate, potassium hydroxide and sodium chloride were supplied by Fischer Scientific, UK. Span 60 (sorbitan monostearate, >97% purity), 1,10-dioctadecyl-3,3,30,30-tetramethylindocarbocyanine perchlorate (Dil), and 3-(4,5-dimethylthiazol-2-yl)-2,5-diphenyl-tetrazoliumbromide (MTT) were provided by Sigma-Aldrich, St. Louis, MO. Tween 80 (polysorbate 80; polyoxyethylene sorbitan monooleate, >97% purity) was purchased from ACROS Organics, Belgium. Water for injection was purchased from Egypt Otsuka Pharmaceutical Co., S.A.E.

2.2. Preparation of vesicles using AA-2G termed glucospanlastics

Plain and drug-loaded glucospanlastics as well as the corresponding conventional spanlastics were fabricated using the ethanol injection method with slight modification.[26,34] The reference conventional spanlastics were comprised of Span 60 and Tween 80 with weight ratio of "4 : 1 w/w". A mixture of solvents (absolute ethanol and chloroform) was chosen to dissolve Span 60 and ITZ (ratio = 1 : 1 v/v; 2 mL). Then, the organic solvent mixture was slowly injected into a Tween 80 solution (10 mL) heated at 60 °C and stirred at 800 rpm for 30 min. Then, the prepared spanlastics were cooled and stirred for 60 min. For the fabrication of glucospanlastics, AA-2G was added to the Tween 80 solution. Different ratios of AA-2G : Tween80 were used with a total weight of 40 mg, while the amount of Span 60 was kept constant (160 mg)

Table 1 Composition of the plain and medicated glucospanlastics containing ascorbyl 2-glucoside AA-2G as a component[a]

Formula code	Tween 80 : AA-2G ratio (w/w)	Drug amount (mg)
$P_{SP}1$	40 : 0	0
$P_{SP}2$	40 : 0	10
$P_{SP}3$	40 : 0	20
$P_{CG}1$	30 : 10	0
$P_{CG}2$	30 : 10	10
$P_{CG}3$	30 : 10	20
$P_{CG}4$	20 : 20	0
$P_{CG}5$	20 : 20	10
$P_{CG}6$	20 : 20	20
$P_{CG}7$	10 : 30	0
$P_{CG}8$	10 : 30	10
$P_{CG}9$	10 : 30	20

[a] All formulae were prepared using fixed amounts of Span 60 (160 mg), Tween 80 : AA-2G ratio was varied (1 : 1, 1 : 3, and 3 : 1), medicated formulae contain 10 and 20 mg ITZ. P_{SP}: preliminary spanlastics and P_{CG}: preliminary component glucospanlastics.

in all formulae. The vesicles were loaded with either 0, 10 or 20 mg of ITZ. The composition of the different preparations is presented in Table 1. For DSC, FTIR and subsequent incorporation in a cream base, lyophilization was performed for the selected formulae using a lyophilizer freeze dryer (Christ: Osterode am Harz, Germany, Alpha 1-2LDplus). The frozen glucospanlastics (−20 °C) were lyophilized at a temperature of −55 °C and pressure of 5 Pa for a 24 h period.

2.3 Characterization of the prepared glucospanlastics

2.3.1 Particle size and polydispersity index measurement. The particle size (PS) and polydispersity index (PDI) of the prepared glucospanlastic vesicles were assessed using a Zetasizer Nano ZS. This approach depicts the mean hydrodynamic diameter of the primary population and PDI, which is a measure of the particle size distribution width, providing insights into the uniformity and monodispersity of the sample. At 25 °C, the samples were measured in triplicate using disposable polystyrene cells (6 runs of 10 cycles).

2.3.2 Zeta-potential ZP measurement. Using capillary zeta cells, the surface charge of the prepared glucospanlastics was determined by estimating their ZP using a Malvern Zetasizer at 25 °C (using deionized water "pH = 6").

2.3.3 Drug content determination. A volume of 200 μL of the prepared glucospanlastics was diluted with 10 mL methanol. The obtained solutions were scanned using a UV/visible spectrometer (UV/visible spectrophotometer: Jasco V630, Japan) at 262 nm. The quantification range was 3.25–25 μg mL^{-1}. The regression equation was found to be $Y = 0.0338x + 0.0907$ and the coefficient of determination (R^2) was found to be 0.999, indicating its good linearity.

2.3.4 Entrapment efficiency (EE%) determination. A dispersion of the ITZ glucospanlastics (2 mL) was centrifugated in Eppendorf Tubes at 15 000 rpm and maintained at a temperature 4 °C for 2 h using a cooling centrifuge. Subsequently, 0.5 mL of the supernatant was separated and the formed pellet was resuspended in 1 mL BPS (pH 7.4) and re-centrifuged. This washing step was performed in triplicate to ensure the removal of free ITZ. Then, the collected supernatant was diluted to 25 mL with methanol and sonicated for 10 min with vigorous shaking. In the obtained pellets, 50 mL of methanol was used to disrupt and dilute the loaded vesicles. The quantity of ITZ in the supernatant and pellets was assessed by UV/visible spectroscopy at 262 nm. The drug entrapment was computed according to the following equation:

$$\mathrm{EE\%} = \frac{\text{entrapped drug}}{\text{total amount of drug}} \times 100$$

2.3.5 Drug loading (DL%) determination. The DL% was calculated according to the following equation:

$$\mathrm{DL\%} = \frac{\text{entrapped drug}}{(\text{total weight of solids})} \times 100$$

2.3.6 Solubilization efficiency (SE%) measurement. Freshly prepared dispersions of the ITZ glucospanlastics were maintained in the refrigerator for 48 h at 4 °C ± 1 °C to speed up the crystallization rate of the unentrapped (free) drug. Then, filtration through a membrane filter (0.45 μm) was performed for a sample from each dispersion to remove the precipitated unentrapped drug. The filtrate was assayed spectrophotometrically at 262 nm. The SE% was determined according to the following equation:

$$\mathrm{SE\%} = \frac{\text{drug content after filtration}}{\text{drug content before filtration}} \times 100$$

The drug concentration in the formulation with SE% greater than 95% was chosen as the optimum one.[35]

2.3.7 Saturation solubility studies. Excess amounts of pure ITZ and ITZ-loaded glucospanlastics containing AA-2G were added separately to 5 mL distilled water and PBS (pH 7.4) in tightly closed 15 mL vials. Then, the vials were left in a thermostatically controlled water bath at 37 °C and shaken at 100 rpm for 24 h.[36] At the end of the specified time, the suspensions were filtered through a Millipore filter (0.45 μm). Then 0.5 mL sample was withdrawn and transferred to a dried porcelain dish. After the obtained solution was completely dried at ambient temperature, residual amounts were dissolved in methanol and exactly diluted to 10 mL and analyzed spectrophotometrically for its ITZ content against the corresponding plain systems as the blank.

2.3.8 Stability study. A one and three-month stability study was carried out to compare the time-dependent variations in the PS, PDI, ZP, EE and DL of the formulations stored at 4 °C. The following formula was used to compute the size change rate and drug leakage:[37]

$$\text{Size change rate } \% = \frac{\mathrm{PS}_{tx} - \mathrm{PS}_{t0}}{\mathrm{PS}_{t0}} \times 100$$

$$\text{Drug leakage } \% = \frac{\mathrm{EE}_{tx} - \mathrm{EE}_{t0}}{\mathrm{EE}_{t0}} \times 100$$

where PS_{t0} and EE_{t0} are the PS and EE% values of the fresh glucospanlastics prepared at day 0 and PS_{tx} and EE_{tx} are the corresponding parameters of the stored formulae (1 and 3 months), respectively. The negligible changes in these parameters (<10%) confirmed the stability of the developed formulae.[7]

2.3.9 Morphological evaluation using transmission electron microscopy (TEM). Selected glucospanlastic vesicles ($P_{CG}2$) were morphologically screened by TEM (JEM-1400 – JEOL, Tokyo, Japan, magnification power: 50 000×) at 80 kV after staining with 1% phosphotungstic acid stain on a C-flat grid. The stained samples were left to dry before inspection.

2.3.10 Differential scanning calorimetry (DSC). Freeze-dried samples of the prepared glucospanlastics were studied by DSC (Shimadzu-DSC 60, Japan; ZEN software) to investigate the thermotropic properties and phase transition behavior of the vesicles. The thermal properties of Span 60, AA-2G, and formulae ($P_{CG}1$, $P_{CG}2$, $P_{CG}3$, and $P_{CG}6$) were investigated. Using dry nitrogen at a flow rate of 30 mL min^{-1}, a precisely measured quantity of sample (3 mg) was enclosed in an aluminum pan with a lid and heated at a rate of 10 °C min^{-1} over the temperature range of 25–350 °C.[38]

2.3.11 Fourier transform infrared "FT-IR" spectroscopy analysis. Infrared spectroscopy (Nicolet 6700, Thermo Scientific, USA; OMNIC software) of each component (ITZ, span 60 and AA-2G) and the final lyophilized formulae; plain and drug loaded ($P_{CG}1$, $P_{CG}2$, $P_{CG}3$, $P_{CG}4$, $P_{CG}5$, and $P_{CG}6$) was performed to analyze the presence of functional groups and the interaction occurring between components after the formation of vesicles. Individual samples were ground with potassium bromide before being pressed to form discs, and their IR spectra (range 4500–400 cm^{-1}) were recorded using an FT-IR spectrophotometer.[39]

2.3.12 Diphenyl-1-picrylhydrazyl (DPPH) antioxidant assay. The DPPH assay was exploited for assessing the antioxidant activity of the proposed glucospanlastics. DPPH is a purple-colored free radical with an absorption maximum of 517 nm. Upon mixing with the tested compounds, DPPH can accept an electron or hydrogen atom from them, leading to its reduction, which is manifested by a discoloration (to pale yellow) and decrease in absorbance to varying degrees based on the competence of the antioxidant potential.[40]

In this investigation, an aliquot of a 0.05% w/v solution of DPPH in methanol was mixed with the chosen glucospanlastic dispersions ($P_{CG}2$ and $P_{CG}5$) and pure AA-2G. Trolox, a synthetic antioxidant that is structurally similar to α-tocopherol, and ascorbic acid (AA) were employed as benchmarks for comparison. The following equation was employed to estimate the percentage of DPPH scavenged:

$$\%\ \text{DPPH} = \frac{(\text{absorbance of stock solution} - \text{absorbance of test solution})}{(\text{absorbance of stock solution})} \times 100$$

Using GraphPad Prism 5®, the antioxidant effect of the studied substances was represented as IC50% (the concentration of the tested substance that causes 50% scavenging of DPPH).

2.3.13 Cytotoxicity assay. To explore the activity of the selected glucospanlastic dispersions $P_{CG}2$ and $P_{CG}3$ and non-formulated ITZ against A431 cells (human squamous carcinoma), the conventional reduction MTT assay was performed. A431 cells (human squamous carcinoma) were seeded in a 96 well plate in medium (Dulbecco modified Eagle's medium +10% fetal bovine serum + 1% streptomycin) for 24 h for growth. Subsequently, the existing culture medium was discarded and replaced with fresh medium and the immersed A431 cells were incubated with various concentrations of the selected glucospanlastics and pure AA-2G as a control for 24 h. After the incubation period, the cells were treated with MTT and the attained formazan crystals were dissolved in DMSO and the absorbance was recorded spectrophotometrically at 570 nm using a microplate reader. The following formula was employed to determine the percentage cell viability:

$$\%\ \text{viable cells} = \frac{\text{absorbance of sample} - \text{absorbance of blank}}{\text{absorbance of control} - \text{absorbance of blank}} \times 100$$

Utilizing the GraphPad Prism® program, the IC50% values, indicating the suppression of growth of 50% cells, were calculated.

2.3.14 *Ex vivo* drug deposition in skin. Visual assessment of the localization and penetrability of the ITZ-glucospanlastic dispersion containing 10 and 20 mg AA-2G ($P_{CG}2$ and $P_{CG}5$, respectively) within skin layers was performed using confocal laser microscopy in comparison to untreated skin as the control.

The abdominal skin of Swiss albino mice weighing 20–25 g was used in this study. The animal was first mercy sacrificed according to the Helsinki arrangement protocol and the guidelines of the Scientific Ethics Committee for Laboratory and Clinical trials at the British University in Egypt, Faculty of Pharmacy, Cairo, Egypt (EX-2315). The abdominal area was carefully shaved and the abdominal skin was excised. The subcutaneous tissue was surgically removed. The full skin specimen was washed with distilled water, wrapped in aluminum foil, and stored in a freezer until use. The prepared skin specimens were soaked in PBS (pH 7.4) for 4 h at room temperature, and then mounted in a Franz diffusion cell between the donor and receptor compartments with the dermal side towards the latter. The receptor compartment was charged with an appropriate volume (12 mL) of PBS (pH 7.4) with 5% Tween 80 to maintain sink conditions, and thus the dermal side of the skin specimen was in direct contact with the medium. The whole assembly was mounted in a thermostatically controlled water bath with the temperature adjusted at 37 °C ± 0.5 °C and stirred at 100 rpm.

Glucospanlastics containing Dil fluorescent dye instead of ITZ were prepared using the ethanol injection method for tracking the penetration of the fluorophore into the different skin layers. After completion of the skin deposition experiments (24 h), the skin was removed, cleaned with PBS pH 7.4 and

mounted on microscope slides for further preparation. The samples were optically sectioned into the z axis to get a 3D reconstruction of the skin using an inverted confocal laser scanning microscope.

2.4 Preparation and evaluation of O/W cream as a matrix for glucospanlastics incorporation

Aiming at prolonging the dermal retention of the glucospanlastics, an O/W cream enclosing the lyophilized glucospanlastics or free drug was formulated (0.1% w/w ITZ). The cream was prepared using the conventional fusion approach. The melted oily component, stearic acid, was mixed with the heated aqueous components (potassium hydroxide, propylene glycol and glycerin) and continually stirred for the formulation of the O/W cream base. The preservative sodium benzoate (0.01%) was also added. After that, 0.1% pure ITZ powder or loaded ITZ in the lyophilized glucospanlastics ($P_{CG}2$) was uniformly dispersed in the cooled cream base.

The evaluation criteria of the O/W cream, including pH, viscosity, occlusive effect and drug content, were previously reported in our previous work.[7] Cream spreadability was determined by taking the glucospanlastic cream in between two slides to dislocate from each other under the influence of a set load. Firstly, a circle (diameter = 2 cm) was marked on one of the slides and 0.5 g of cream placed in it.[41,42] Then, the other slide was inserted on the top of the formulation and a weight of 0.5 kg was applied on the upper slide for 5 min. The increase in diameter was recorded as an indicator of the cream spreadability. The spreadability was determined using the following equation:

$$\%\ \text{spreadability} = \frac{D_f}{D_i} \times 100$$

where D_i is the initial diameter (2 cm) and D_f is the final diameter after spreading.

Regarding extrudability, the prepared glucospanlastics cream was filled in a collapsible tube and pressure from a finger was applied. The quantity of the cream extruded through the opening of the tip following the application of pressure was weighed and the percentage of extrudability was calculated.[7,43]

2.5 *In vivo* anticancer efficacy using Ehrlich carcinoma model

The effectiveness of the various glucospanlastic formulations in treating cancer was evaluated in female Swiss albino mice (aged 8–10 weeks and weighing between 20–24 g) employing a procedure similar to that previously described, with slight modifications.[7] The experiments were conducted in accordance with the Helsinki arrangement protocol and the guidelines of the Scientific Ethics Committee for Laboratory and Clinical Trials approved by The British University in Egypt (EX-2315). Ehrlich ascites carcinoma cells, obtained from female Swiss mouse donors sourced from the Egyptian National Cancer Institute at Cairo University, were aseptically isolated and suspended in sterile isotonic saline solution. A cohort of thirty-six mice was subjected to randomization and housed in a carefully controlled atmosphere set at ambient temperature with 50% relative humidity. The mice were given *ad libitum* access to food and water throughout the experimental period. To induce the solid tumor, a suspension of 2.5×10^6 viable cells in 0.1 mL of normal saline was subcutaneously injected into the upper dorsal region of the left hind leg. After 12 days, the induced tumor reached the appropriate size of 100–120 mm^3. The hair on the skin of the animals was shaved above the tumor site. Subsequently, the topical administration of distinct treatments commenced in accordance with the predetermined experimental protocol. The glucospanlastic formulations were freeze-dried (Eyela FDU-2100, Japan) and incorporated into an oil-in-water (O/W) cream base, enabling their easy application onto the skin of the animals at a concentration of 0.1% w/w of ITZ. The prepared cream base used in this study was characterized using the same procedure as described in our previous research.[7] Notably, a modification was performed to include sodium benzoate as a preservative.

Consequently, the animals were subjected to random allocation into six groups, each consisting of six animals, according to the following grouping scheme:

Group I (cancerous untreated control group) received standard provisions of food and water without any additional treatment after the subcutaneous solid tumor was induced.

Group II (conventional ITZ cream group) received topical administration of a 0.1% ITZ cream (0.5 g) twice daily.

Group III ($P_{CG}1$, plain formula containing 10 mg ascorbyl glucoside) received topical (0.5 g) cream twice daily.

Group IV ($P_{CG}4$, plain formula containing 20 mg ascorbyl glucoside) received topical (0.5 g) cream twice daily.

Group V ($P_{CG}2$, drug loaded formula containing 10 mg ascorbyl glucoside and 10 mg ITZ) received topical (0.5 g) cream twice daily.

Group VI ($P_{CG}5$, drug loaded formula containing 20 mg ascorbyl glucoside and 10 mg ITZ) received topical (0.5 g) cream twice daily.

All treatments were meticulously applied with a rubbing action directly on the tumor site. The body weights of the mice were recorded daily following the initiation of treatment to assess and compare the differences in weight gain between the groups receiving treatment and the untreated control group. Daily at specific times, the tumors were visually inspected and their volumes were quantified using digital Vernier calipers (Prokit's Industries Co., Ltd, Taiwan, ROC). The solid tumor volume was estimated using the following equation:[44]

$$\text{Tumor volume} = \text{length} \times \text{width}^2 \times 0.52$$

The study was terminated on day seventeen from the start of the experiment after reaching the tumor volume of 500 mm^3 in group I, and the mice were euthanized by cervical dislocation after 8 h from the last application of the treatment. Then, the formed tumor masses were removed and weighed for subsequent analysis.

2.5.1 *In vivo* histopathological study. The excised tumor masses were collected and preserved in 10% buffered formalin for subsequent histopathological examination. Tissues with

a thickness of approximately 4 μm were obtained from the various samples utilizing a rotary microtome and affixed onto glass slides. For comprehensive morphological evaluation, the tissue sections were subjected to staining with hematoxylin and eosin, which is the standard method employed for general histopathological examination. Subsequently, the stained slides then subjected to blinded light microscopic examination. All standards protocols for sample fixation and staining were diligently executed following the methodology outlined by Waz *et al.* 2021.[45] To evaluate the antiproliferative activity and confirm the findings of the histopathological images quantitively, necrosis percentage was investigated in all groups. Morphological measurements and data analysis were performed utilizing the Leica Application module, which is a software module designed for tissue section analysis. This module was integrated with a high-definition (HD) microscopic imaging system (Leica Microsystems GmbH, Germany). The combined setup facilitated the acquisition of precise morphological measurements and the analysis of the obtained data.[46]

2.5.2 Biochemical assessment of antioxidant markers in tumor mass. Prior to the dissection process, the samples were washed with a pH 7.4 phosphate-buffered saline (PBS) solution containing 0.16 mg mL^{-1} heparin. This step aimed to eliminate any residual red blood cells and clots from the samples. Subsequently, the samples were homogenized (using Potter-Elvehjem homogenizer) in a cold "0–4 °C" buffer (50 mM potassium phosphate, pH 7.5) at a ratio of 5–10 mL per g of tissue. Following homogenization, the samples were subjected to centrifugation at 4000 rpm for 15 min.[47,48] The levels of the antioxidant indices, including malondialdehyde (MDA), total antioxidant capacity (TAC), and glutathione (GSH), were determined in the resulting homogenates using a commercially available assay kit (Biodiagnostic, Cairo, Egypt).

2.6 Statistical analysis

All values are expressed as the mean of three experiments ± standard deviation (SD). The Student's *t*-test or ANOVA was employed for comparison of the mean values using the GraphPad Prism® software version 5 and considered significant when p value ≤ 0.05.

3. Results and discussion

3.1. Preparation of vesicles using AA-2G termed glucospanlastics

To the best of our knowledge, AA-2G has not been utilized in the preparation of nanovesicular systems. Accordingly, the preparation of spanlastics as a newer generation of surfactant-based vesicles that are made of Span 60 and edge activators was attempted. Based on earlier reports,[34,49] a constant Span 60 : Tween 80 ratio of "4 : 1" was used in the preparation of all formulae by the ethanol injection method, which has been well-documented to produce nanovesicles with narrow size range.[50] Specifically, this ratio was found to be the optimum ratio between the bilayer forming surfactant 'Span 60' and the edge activator 'Tween 80' for the formation of small-sized vesicles. Besides, the fabrication of compact small vesicles has been well-linked to the selection of Tween 80 as the edge activator amongst other edge activators such as Cremophore RH 40 and Tween 20.[26,51–53] Firstly, when preparing spanlastics using AA-2G instead of Tween 80, no colloidal dispersion was attained. The well-documented high hydrophilicity of AA-2G[54] may be responsible for the necessity of the Tween 80 entity in the design of spanlastics. Specifically, the hydrophilic AA-2G failed to perform the function of edge activator in spanlastics, pinpointing the relevance of edge activators in producing spanlastics. The hydrophobicity of the edge activator is well-reported to destabilize the vesicular membrane, leading to the fluidization of spanlastics.[55]

Consequently, we employed the conventional spanlastics with its referenced composition of Span 60 and Tween 80. As an innovative approach, AA-2G was incorporated in the spanlastic composition. The vesicles were successfully prepared, showing no signs of precipitation or aggregation.

3.2. Characterization of the prepared glucospanlastics

All the component glucospanlastics showed a particle size in the nanorange (137.7–454.4 nm, Table 2). In addition, they were mono-dispersed and uniform in size, as indicated by their PDI values (0.25–0.50). This highlighted the homogeneity of the system and reproducibility of the preparation method.[56] Moreover, the ZP, EE%, DL% and SE% of all the investigated glucospanlastics were in the range of (−23.5 to −38.2 mV), (95.9–99.4%), (4.03–8.49%), and (40.2–97.2%), respectively.

Interestingly, varying the ratio between Tween 80 and AA-2G had a considerable effect on PS. Comparing the plain AA-2G-free spanlastics "$P_{SP}1$" to glucospanlastic formulae $P_{CG}1$, $P_{CG}4$, and $P_{CG}7$, regardless of the amount of AA-2G, it was observed that decreasing the amount of Tween 80, while increasing the amount of AA-2G yielded larger vesicles (PS values: 100.6 ± 7.61 *versus* 137.7 ± 5.42, 203.9 ± 2.81, 314.7 ± 3.42 nm; $p < 0.05$), respectively. Similar trends were observed in the drug-loaded formulae. This can be attributed to the fact that as an edge activator, Tween 80 has been reported to reduce the interfacial tension, which facilitates the partition, increasing the emulsification and formation of smaller vesicles.[49,57] Besides, the less bulky nature of Tween 80 due to the presence of unsaturation could facilitate its incorporation in the nanovesicles, resulting in a lower PS.[58] Thus, increasing the amount of AA-2G at the expense of the amount of Tween 80 may lead to the formation of larger vesicles. However, all the prepared glucospanlastics still possessed nano-dimensions below 500 nm.

Zeta potential is considered a relevant criterion for the characterization of nanoplatforms owing to its impact on the stability of nanocarriers, and hence the *in vivo* fate of the incorporated drugs.[59,60] Table 2 shows the negative surface charge of the proposed glucospanlastics (around −30 mV), which was dependent on the amount of edge activator "Tween 80". The magnitude of ZP of the plain conventional spanlastics $P_{SP}1$ (ZP = −36.5 ± 1.4 mV) was significantly higher than that of the AA-2G-containing spanlastics ($P_{CG}1$, $P_{CG}4$, and $P_{CG}7$; with values of −27.1 ± 0.43, −25.3 ± 1.22 and −23.5 ± 0.72 mV; $p <$

0.05), respectively. Similarly, the magnitude of ZP of the drug-loaded formulae decreased with an increase in the content of AA-2G relative to that of Tween 80. $P_{SP}1$ and $P_{SP}3$ showed a significantly higher negative surface charge (ZP = −38.7 ± 3.2 and −39.2 ± 1.4 mV, respectively) than the other formulae ($P_{CG}2$, $P_{CG}3$, $P_{CG}5$, $P_{CG}6$, $P_{CG}8$ and $P_{CG}9$; $p < 0.05$). Analogous negative surface charges were reported earlier for conventional spanlastics.[61] The presence of the hydroxyl group of Span 60 could create a high intensity of negative charges on the vesicular exterior.[62] Comparable negative surface charges have been documented previously for ITZ-loaded spanlastics made of Span 60 and Tween 80.[63] In particular, Tween 80-based spanlastics have been found to possess a more negative charge than their Tween 40-based counterparts.[52]

In the case of the EE% and DL% of the prepared formulae, the effect of the tested variables (different ratios of Tween 80 : AA-2G and two different drug amounts) on these parameters is shown in Table 2. The percentage of drug entrapped and its loading in conventional spanlastics (lacking AA-2G; $P_{SP}2$) containing 10 mg ITZ were found to be 88.2 ± 0.1% and 4.19 ± 0.34%, respectively, indicating the high affinity of ITZ to the nanoplatform. However, the further incorporation of ITZ reaching its double amount (20 mg) in spanlastics "$P_{SP}3$" was accompanied with a concomitant significant reduction in ITZ entrapment (60.21 ± 1.3%; $p < 0.05$) with no notable change in the ITZ loading (4.83 ± 0.34%; $p > 0.05$). This is consistent with the study by El Meshad *et al.*, who reported that the lower ITZ EE of spanlastics containing the higher ITZ amount of 20 mg can be attributed to the saturation of the fabricated vesicles with drug and any further increment in drug amount would result in its precipitation.[63]

Interestingly, replacing a certain amount of Tween 80 with AA-2G in the ratio of 3 : 1, 1 : 1, 1 : 3 ($P_{CG}2$, $P_{CG}5$ and $P_{CG}8$, respectively; containing 10 mg ITZ), led to the corresponding increase in ITZ EE% with relatively constant DL% values compared to that of the AA-2G-free spanlastics; $P_{SP}2$; ($p < 0.05$). The decrease in the amount of Tween 80 amount in these vesicles can be responsible for their decreased fluidization. The lower the fluidization of the spanlastics, the lower the drug leakage, as reported earlier.[49,64] Moreover, doubling the amount of ITZ to 20 mg in formulae $P_{CG}3$, $P_{CG}6$ and $P_{CG}9$ resulted in an increase in EE% and drug loading in the range of 1.59–1.62- and 1.69–1.75-fold, respectively, compared with the AA-2G-free spanlastics containing the same amount of ITZ ($P_{SP}3$; $p < 0.05$). These findings indicated the competence of the AA-2G-containing spanlastics in entrapping a higher amount of ITZ, performing the desired ITZ solubilization.[4,65] According to the literature, incorporating ITZ in NPs based on mPEG-*b*-PLA copolymer led to the encapsulation and loading of appreciable ITZ amounts (99.40% ± 0.53% and 3.82% ± 0.02%, respectively) owing to its enhanced solubilization.[66] It is worth mentioning that elevating the amount of AA-2G from 10 mg to 30 mg yielded a slight decrease in EE value, although not to a statistically relevant level ($p > 0.05$). This can be explained by the possible complexation *via* the formation of a hydrogen bond between the amine or triazole group in ITZ and the hydroxyl group in AA-2G (which will be addressed later in the FTIR study).

The solubilization efficiency can exactly determine the optimum concentration of drug that the vesicles can entrap effectively.[35] As revealed in Table 2, the SE of formulae $P_{SP}1$ and $P_{SP}2$ was <95%, indicating the low solubilization efficiency of the conventional AA-2G-free spanlastics containing only Tween 80. In contrast, it was observed that the presence of AA-2G in the $P_{CG}2$, $P_{CG}5$ and $P_{CG}8$ formulae containing 10 mg ITZ led to a marked increase in the solubilization efficiency, reaching the optimum values (>95%), while in their counterparts containing 20 mg ITZ ($P_{CG}3$, $P_{CG}6$, and $P_{CG}9$), the SE values became <95%, indicating the crystallization of ITZ. This may be related to its hydrophobic nature ($\log p = 5.70$).

Based on the aforementioned premises, the nano-sized and colloidally stable glucospanlastics containing AA-2G as a component were successfully prepared and were capable of accommodating 20 mg drug. In particular, $P_{CG}2$ (Fig. S2†) considerably satisfied the requisites of an effective topical delivery system with respect to nano-dimensions, colloidal stability, maximum payload (>99%) and optimum drug solubilization efficiency (>95%). Therefore, it was subjected to further investigations to explore its suitability as an antioxidant nanoplatform for the topical delivery of anticancer drugs (*i.e.*,

Table 2 Characterization of the plain and medicated glucospanlastics containing ascorbyl glucoside as a component[a]

Formula code	PS (nm)	PDI	Zeta potential (mV)	EE (%)	DL (%)	SE (%)
$P_{SP}1$	100.6 ± 7.61	0.23 ± 0.08	−36.5 ± 1.40	—	—	—
$P_{SP}2$	223.8 ± 0.98	0.50 ± 0.05	−38.7 ± 3.21	88.2 ± 0.10	4.19 ± 0.21	87.3 ± 1.22
$P_{SP}3$	338.4 ± 1.69	0.46 ± 0.07	−39.2 ± 1.41	60.2 ± 1.30	4.83 ± 0.34	40.2 ± 0.51
$P_{CG}1$	137.7 ± 5.42	0.29 ± 0.01	−27.1 ± 0.43	—	—	—
$P_{CG}2$	286.0 ± 4.25	0.41 ± 0.06	−35.6 ± 0.62	99.4 ± 1.02	4.23 ± 0.02	97.2 ± 1.11
$P_{CG}3$	414.0 ± 9.41	0.49 ± 0.07	−38.2 ± 0.212	97.8 ± 0.81	8.49 ± 0.81	87.2 ± 2.10
$P_{CG}4$	203.9 ± 2.81	0.25 ± 0.01	−25.3 ± 1.22	—	—	—
$P_{CG}5$	404.5 ± 3.12	0.45 ± 0.08	−31.9 ± 0.35	98.8 ± 0.64	4.20 ± 0.26	95.5 ± 0.70
$P_{CG}6$	430.3 ± 6.43	0.44 ± 0.04	−33.6 ± 0.49	96.4 ± 0.52	8.20 ± 0.04	88.2 ± 1.91
$P_{CG}7$	314.7 ± 3.42	0.32 ± 0.05	−23.5 ± 0.72	—	—	—
$P_{CG}8$	425.9 ± 2.31	0.43 ± 0.02	−30.8 ± 0.32	97.2 ± 0.32	4.32 ± 0.07	95.1 ± 0.82
$P_{CG}9$	454.4 ± 7.21	0.48 ± 0.03	−32.8 ± 1.55	95.9 ± 0.41	8.41 ± 0.14	81.2 ± 1.71

[a] All formulae were prepared using a fixed amount of Span 60 (160 mg), Tween 80 : AA-2G mixture of 40 mg ratio was varied (1 : 1, 1 : 3, and 3 : 1), medicated formulae contain 10 and 20 mg ITZ. P_{SP}: preliminary spanlastics and P_{CG}: preliminary component glucospanlastics.

antioxidant potential, cytotoxic effect and skin permeation). To deeply investigate the solid state of ITZ in the proposed vesicles, the possible interaction between AA-2G and ITZ on the one hand, and interaction with the vesicle components on the other hand and the functional features of the $P_{CG}2$ vesicles were compared with other plain and drug-loaded formulae, containing a higher drug amount, higher AA-2G amount, or both.

3.2.1. Saturation solubility study. The saturation solubility values of the non-formulated ITZ and $P_{CG}2$ were determined. ITZ is reported to have the aqueous solubility of 1 ng mL^{-1} and 5 μg mL^{-1} at pH 7 and pH 1, respectively.[67] This can explain the inability to detect it in very small quantities by UV analysis (no peak was determined). Obviously, the solubility of ITZ was greatly enhanced when it was incorporated in the glucospanlastics, showing >100 μg mL^{-1} in water and PBS pH 7.4 (136 ± 0.74, and 465 ± 0.14 μg mL^{-1}), respectively. Interestingly, a 3.42-fold increase in the saturation solubility of the ITZ nanoform was noticed in PBS. The enhancement in its saturation solubility was found to be well-linked to its nanonization according to the Ostwald–Freundlich equation, stating that smaller particles dimensions are accompanied with higher solubility.[68] This can be attributed to the fact that AA-2G mainly acts as a solubilizing agent, possessing high solubilization power, as stated earlier. The formation of a bond between the amide group (N–H) group present in ITZ and OH– group present in AA-2G may be responsible for the enhanced solubility.[69]

3.2.2. Stability study. The stability study was performed to explore the possible drug leakage and the variations in vesicles size over specific storage periods (1 and 3 months). Over these storage periods, the investigated spanlastics and glucospanlastics showed a size change rate of <4% ($p > 0.05$) and statistically irrelevant decline in EE% and DL% values (<1% of drug leakage), as shown in Table S1.† The results displayed that the innovative glucospanlastics showed acceptable variations in the tested parameters of <10%,[70] highlighting their remarkable stability.

3.2.3. Morphological examination using transmission electron microscopy (TEM). The TEM images of the selected glucospanlastics formula $P_{CG}2$ showed the presence of uniform, smooth and well-dispersed spherical vesicles with no aggregation (Fig. 2). The PS of $P_{CG}2$ determined by TEM was 75.51 ± 15.00 nm. The significant reduction in PS using the TEM technique compared to that obtained using the DLS technique can be attributed to the fact that the DLS technique measures the average hydrodynamic PS in aqueous medium, whereas the TEM technique measures the true PS of the sample under dry condition.[71]

3.2.4. Differential scanning calorimetry (DSC). The DSC thermograms of ITZ, Span 60, AA-2G, plain glucospanlastics containing 10 mg AA-2G ($P_{CG}1$), and drug-loaded glucospanlastics containing 10 mg ITZ ($P_{CG}2$) are presented in Fig. 3. For comparison, both glucospanlastics containing a higher ITZ amount (20 mg) with the same AA-2G amount ($P_{CG}3$) and that containing higher amounts of ITZ and AA-2G of 20 mg each ($P_{CG}6$) were thermally analyzed in Fig. 3.

The DSC thermograms of Span 60 and AA-2G presented endothermic peaks at 59.36 °C and 172.8 °C, respectively. A distinct endothermic peak at 170 °C, which corresponds to the melting point of pure ITZ, was visible in the DSC thermogram of ITZ. This result is consistent with the data in the literature.[7,72–74] Interestingly, the disappearance of the AA-2G endothermic peak and shifting of the endothermic peak of Span 60 to 55.25 °C in the thermogram of the plain-glucospanlastics containing 10 mg AA-2G ($P_{CG}1$) indicate the formation of the glucospanlastics, the interlinkage of AA-2G and the vesicles components and their association within the vesicles. The shift in the endothermic peak of Span 60 in conventional spanlastics was previously reported.[63] Further, the DSC thermogram of the ITZ-glucospanlastics containing 10 mg AA-2G and 10 mg ITZ ($P_{CG}2$) displayed the disappearance of the distinctive endothermic peaks of ITZ and AA-2G, indicating the amorphization of ITZ, and hence its improved solubilization.

To investigate the link between the presence of AA-2G and the boosted loading capacity of the vesicles, formulae $P_{CG}3$ and $P_{CG}6$ containing 10 mg and 20 mg AA-2G, respectively, and a fixed ITZ amount of 20 mg were investigated. The DSC thermogram of $P_{CG}3$ showed the disappearance of the endothermic peaks of either ITZ or AA-2G, whereas, in the formula containing high amounts of both ITZ and AA-2G ($P_{CG}6$), it displayed the presence of an endothermic peak at 168.38 °C, but its intensity was lower relative to peaks of ITZ and AA-2G.

To elucidate if this peak corresponded to ITZ or AA-2G, FT-IR was performed for these formulae in particular, as will be addressed in the following section.

3.2.5. Fourier transform infrared (FT-IR) spectroscopy analysis. FT-IR analysis is a very effective tool utilized to demonstrate the characteristic peaks of distinct functional groups in the studied materials. In addition, the possible interactions in the prepared formulae can be elucidated using FT-IR.[75,76] The selected formulae of $P_{CG}1$, $P_{CG}2$, $P_{CG}3$, $P_{CG}4$, $P_{CG}5$, and $P_{CG}6$ and their individual components ITZ, Span 60 and AA-2G were analyzed using FTIR spectroscopy and the corresponding spectra are demonstrated in Fig. 4.

The FT-IR spectrum of ITZ displayed characteristics absorption bands of [CH aromatic at 3068 cm^{-1} and 3129 cm^{-1}], [C=C and C=N at 1551 cm^{-1} and 1614 cm^{-1}], [C–N stretching, C=O amide at 1184 cm^{-1} and 1699 cm^{-1}], and [CH alkane at 2823 cm^{-1} and 2965 cm^{-1}], respectively. These peaks are consistent with previous reports.[77–79] The spectrum of Span 60 showed [C=O ester stretching at 1735 cm^{-1}], [C–CO–C stretching at 1179 cm^{-1}], [CH alkane at 2918 cm^{-1} and 2850 cm^{-1}], and [OH-stretching at 3410 cm^{-1}], as previously observed.[80] The spectrum of AA-2G displayed characteristic peaks corresponding to C=O stretching at 1701 cm^{-1} and 1769 cm^{-1} and a broad –OH peak at 3490 cm^{-1}.[16,81]

The FT-IR spectrum of the plain glucospanlastics P_CG1 and P_CG4 (containing 10 and 20 mg AA-2G, respectively) showed the characteristics bands of Span 60 and AA-2G. However, these peaks had lower intensities compared with that of the individual components. The formation of a vesicular system was reported to be responsible for the lower intensity of these bands.[82]

In the drug-loaded formulae ($P_{CG}2$ and $P_{CG}5$), the observed slight shifting and disappearance of the characteristics peaks of ITZ was obvious. This can be attributed to the possible

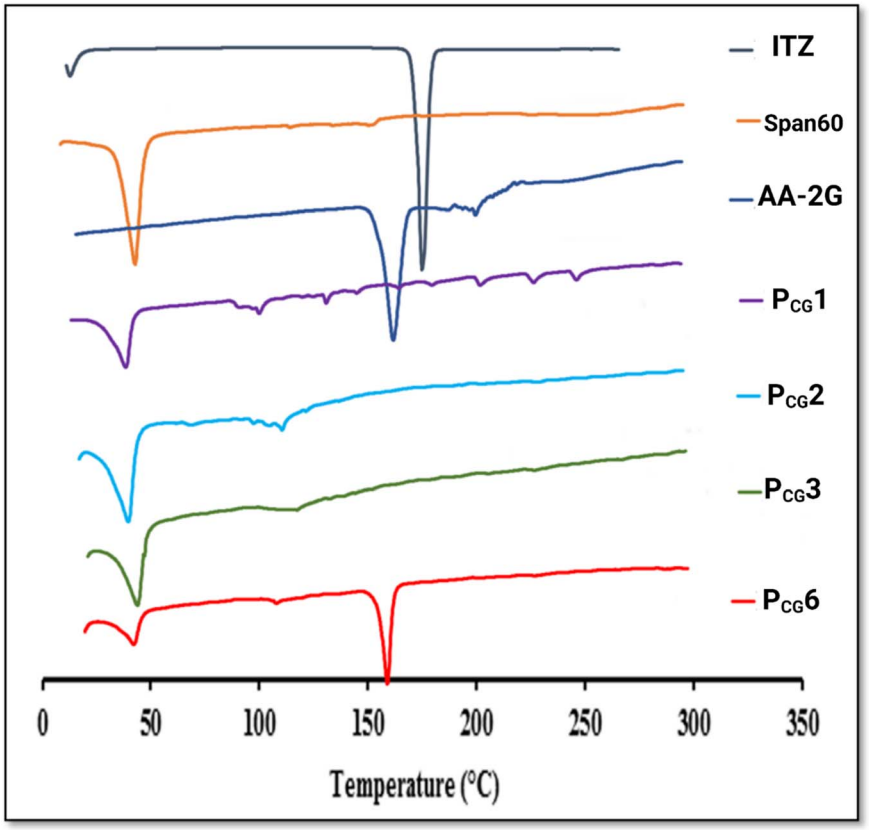

Fig. 3 Differential scanning calorimetry (DSC) thermograms of ITZ, Span 60, ascorbyl glucoside AA-2G, $P_{CG}1$, $P_{CG}2$, $P_{CG}3$, and $P_{CG}6$. $P_{CG}1$: plain glucospanlastics containing 10 mg AA-2G. $P_{CG}2$: ITZ-glucospanlastics containing 10 mg AA-2G and 10 mg ITZ. $P_{CG}3$: ITZ-glucospanlastics containing 10 mg AA-2G and 20 mg ITZ. $P_{CG}6$: ITZ-glucospanlastics containing 20 mg AA-2G and 20 mg ITZ.

interaction (complexation between AA-2G and ITZ) *via* the reaction between the hydroxyl group of AA-2G and amine or triazole group of ITZ improving both its nanoencapsulation and nanovesicle stability. This is in good agreement with previous studies.[66,83]

In contrast, in the drug-loaded formulae $P_{CG}3$ and $P_{CG}6$, the peaks of ITZ were still visible, but with a lower intensity, confirming the decrease in the solubilization efficiency and entrapment observed in these formulae. Referring to the DSC findings of the aforementioned formulae, the FT-IR findings confirm that the endothermic peak located at 168.38 °C corresponds to ITZ. It is worth noting that peaks of AA-2G disappeared in both the plain and drug-loaded formulae, highlighting the possibility of its interaction with Span 60 and Tween 80 during the formation of the bilayer vesicle. This can explain the increment in ITZ entrapment in the AA-2G-based spanlastics relative to their counterparts lacking AA-2G.

3.2.6. Diphenyl-1-picrylhydrazyl (DPPH) antioxidant assay. The most popular approach to assess the antioxidant potential of assorted compounds is the DPPH scavenging assay. Thus, the reaction with the DPPH free radical was used to test the *in vitro* scavenging efficacy of pure AA-2G and $P_{CG}2$. To elucidate the impact of the antioxidant, AA-2G, the formula containing a higher AA-2G amount (20 mg), keeping the amount of ITZ fixed at 10 mg, $P_{CG}5$, was also investigated.

Non-formulated ITZ had no antioxidant performance (IC50% value > 500 μg mL^{-1}), whereas the non-formulated AA-2G showed a good IC50% value (67.2 ± 5.23 μg mL^{-1}) compared to that of ascorbic acid and Trolox (25.41 ± 0.71 and 24.42 ± 0.87 μg mL^{-1}, respectively), as shown in Fig. 5. The glucospanlastics were found to exhibit antioxidant activity that was well-linked to the content of AA-2G. In formulae $P_{CG}2$ containing (10 mg AA-2G) and $P_{CG}5$ (20 mg AA-2G), their IC50% values were found to be 49.02 ± 2.37 and 61.32 ± 4.19 μg mL^{-1}, respectively. These findings indicate that the presence of the antioxidant AA-2G inside the glucospanlastics did not alter its free radical scavenging competence, substantially yielding antioxidant vesicles.[8,84,85]

3.2.7. Cytotoxicity assay. The cytotoxicity of the ITZ-glucospanlastics containing two different concentrations of ITZ, 10 mg and 20 mg ($P_{CG}2$, $P_{CG}3$, respectively), in comparison with pure ITZ and pure AA-2G in the concentration range of 0.01–100 μg mL^{-1} of ITZ was assessed using A431 cells *via* the MTT assay. The cell viability and IC50 scores are presented in Fig. 6. As stated earlier in our paper,[7] the IC50 value of pure-ITZ is 13.07 ± 0.82 μg mL^{-1}, highlighting its cytotoxicity. Notably, the ITZ-glucospanlastic formulations $P_{CG}2$ and $P_{CG}3$ reduced the IC50 of pure ITZ by 1.3 and 5.06-fold (9.997 ± 0.5 and 2.581 ± 0.13 μg mL^{-1}; $p < 0.05$), respectively. As expected, the higher the ITZ amount, the lower the IC50 value. This significant increase in the cytotoxic activity of the ITZ-glucospanlastics can

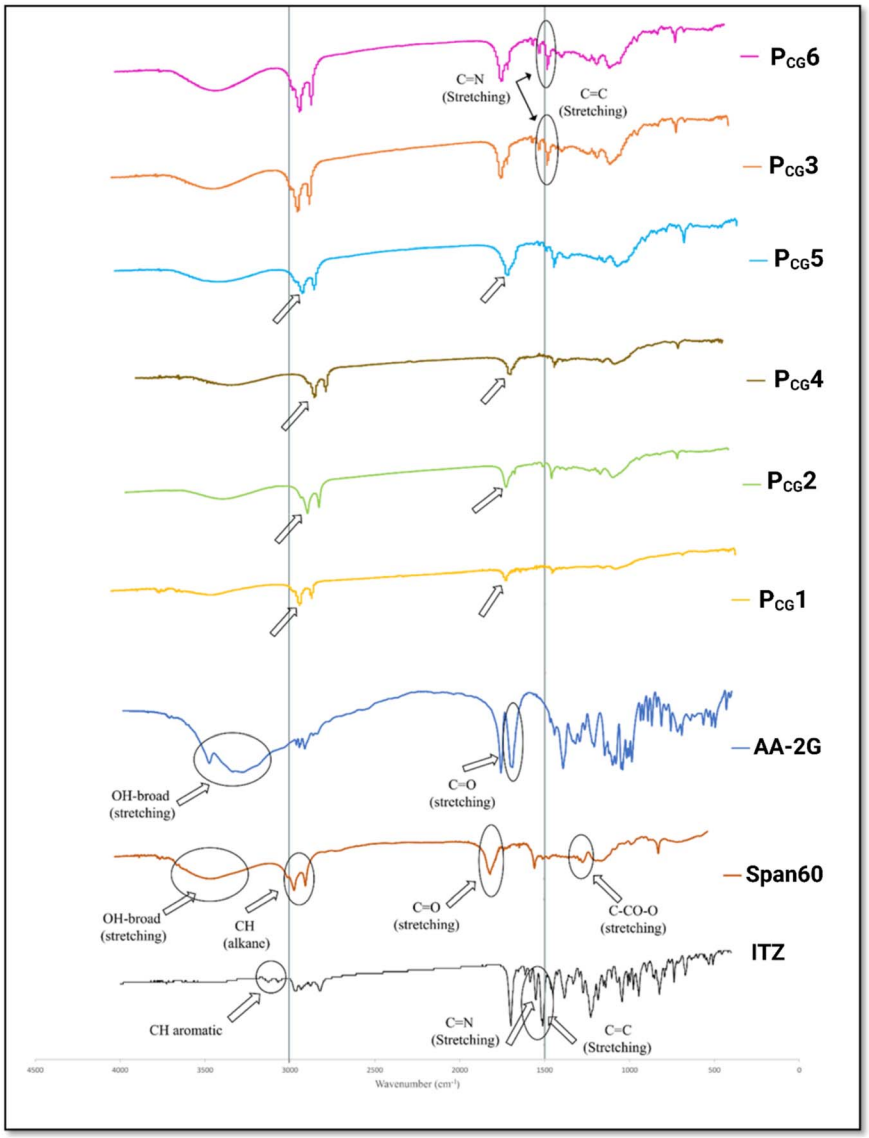

Fig. 4 FT-IR spectra of itraconazole, Span 60, ascorbyl glucoside, $P_{CG}1$, $P_{CG}2$, $P_{CG}3$, $P_{CG}4$, $P_{CG}5$ and $P_{CG}6$. $P_{CG}1$: plain glucospanlastics containing 10 mg AA-2G. $P_{CG}2$: ITZ-glucospanlastics containing 10 mg AA-2G and 10 mg ITZ. $P_{CG}3$: ITZ-glucospanlastics containing 10 mg AA-2G and 20 mg ITZ. $P_{CG}4$: plain glucospanlastics containing 20 mg AA-2G. $P_{CG}5$: ITZ-glucospanlastics containing 20 mg AA-2G and 10 mg ITZ. $P_{CG}6$: ITZ-glucospanlastics containing 20 mg AA-2G and 20 mg ITZ.

be attributed to the small size of the nano formulation, enhancing their intracellular uptake, and hence their cytotoxic effect.[86,87] It is worth noting that pure AA-2G exhibited an inhibitory effect on the proliferation of A431 cells (IC50 = 167.3 ± 8.39 μg mL^{-1}), showing moderate cytotoxicity according to the above-mentioned values (IC50 range = 100–1000 μg mL^{-1}).[88]

3.2.8. *Ex vivo* drug deposition in skin. In this study, the deposition of ITZ-loaded glucospanlastics containing two different amounts of AA-2G ($P_{CG}2$ and $P_{CG}5$ containing 10 and 20 mg AA-2G, respectively) was evaluated qualitatively using confocal scanning laser microscopy (CLSM). To mimic the presence of ITZ in the glucospanlastic vesicles, the lipophilic Dil dye ($\log p = 20$) was utilized, ensuring its high entrapment in the vesicles, low dispersal in aqueous solution and stability.[89]

Microscopic visualization of cross-sectional skin cuts using confocal laser scanning microscopy was performed. After applying the fluorescently labeled formulas for 24 h, the fluorescence intensity and depth of penetration of the Dil dye within different skin strata were measured.

The untreated skin exhibited no autofluorescence score (Fig. 7(A)). In contrast, Fig. 7(B) and (C) show the distribution of the Dil-loaded glucospanlastics, which contained 10 mg AA-2G ($P_{CG}2$) and 20 mg AA-2G ($P_{CG}5$), respectively, in the different mice skin strata. It is noticeable that both formulae accumulated deeply into the skin layers, yet a higher significant intensity ($p < 0.05$) was noticed in skin layers in the case of the Dil-loaded glucospanlastics containing 20 mg AA-2G, $P_{CG}5$, compared with that containing 10 mg AA-2G, $P_{CG}2$, (values for stratum corneum, epidermis and dermis were 34.98 ± 3.39 pixel

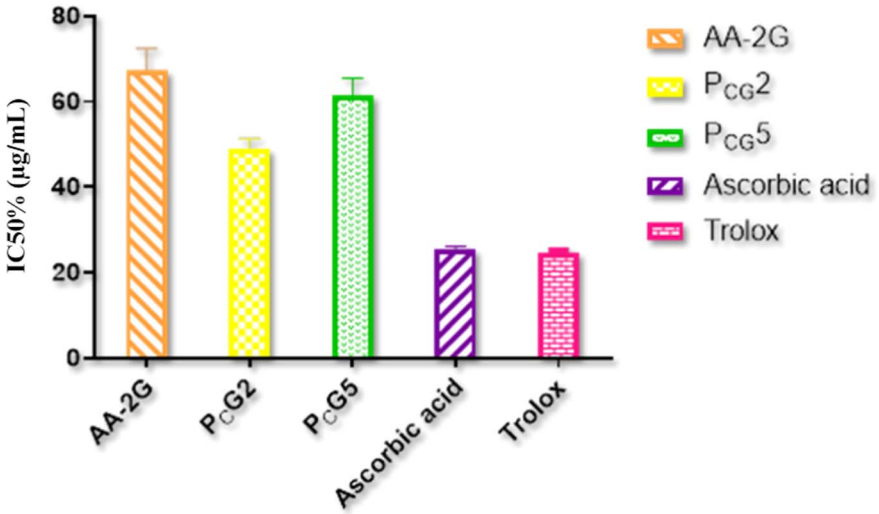

Fig. 5 DPPH free radical scavenging potential of glucospanlastic dispersions using ascorbic acid and Trolox as references. Results are expressed as mean ± SD. $P_{CG}2$: ITZ-glucospanlastics containing 10 mg AA-2G and 10 mg ITZ. $P_{CG}5$: ITZ-glucospanlastics containing 20 mg AA-2G and 10 mg ITZ.

per μm^2, 76.86 ± 5.84 pixel per μm^2 and 87.36 ± 2.34 pixel per μm^2 for $P_{CG}5$ *versus* 80.41 ± 1.98 pixel per μm^2, 21.41 ± 1.23 pixel per μm^2 and 20.52 ± 3.20 pixel per μm^2 for $P_{CG}2$), respectively.

These findings indicate the boosted permeation of both glucospanlastics containing 10 mg and 20 mg AA-2G through the mouse skin, with the latter being superior ($P_{CG}5$). The greater degree penetration of the Dil-loaded glucospanlastics containing 20 mg AA-2G was probably due to higher fusion of the glucospanlastic content with the cutaneous layers, allowing their disruption and heightened fluidity. Consequently, their distribution through the interstitial cutaneous gaps and internalization in deeper skin strata could be accomplished.

3.3. Preparation and evaluation of O/W cream as a matrix for the incorporation of glucospanlastics

Regarding the cream assessment, the cream formulation demonstrated favorable characteristics, including appropriate consistency, aesthetically pleasing homogeneity, absence of grittiness (smooth texture), appealing odor, and visually attractive whitish color. The average pH value of the cream was determined to be 6.94 ± 0.31, indicating an acceptable range that minimizes the risk of skin irritation upon application. This finding confirms the suitability of the cream for topical use, given that its pH closely aligns with the physiological pH of the skin, ensuring the good tolerability of the cream.[90] The prepared cream also demonstrated satisfactory drug content values of 97.12% ± 0.25%, providing evidence that the active ingredient, ITZ, was uniformly distributed within the cream matrix. It also possessed high spreadability and extrudability values of 542.5% ± 6.5% and 98.2% ± 0.90%, respectively, with pseudoplastic (shear-thinning) behavior, facilitating its topical application, covering greater skin surface and promoting the available area for drug permeation.[91]

3.4. *In vivo* anticancer efficacy using Ehrlich carcinoma model

Experimentally, Ehrlich tumor cells are substantially utilized for the elucidation of the antitumor effectiveness of various drugs and that enclosed in nanoplatforms. This is due to the facility and promptness of both their implantation in mice, regardless of their strain, and their development and recession. Besides, the duration of the *in vivo* experiment was greatly shortened compared to other approaches of cancer modeling.[92] Accordingly, the formation of apparent and rapidly developed solid tumors can be noticed.

The formation of a solid tumor was initiated by the subcutaneous injection of EAC cells into the upper dorsal area of the left hind leg. The tumor induction method was effective and verified, as stated in our previous report.[7] All the groups achieved an appreciable tumor volume (more than 100 mm^3) within nine days following the subcutaneous injection of cancer cells. Subsequently, the treatments were administered by applying 0.5 g of cream twice daily for the following eight days.

It should be noted that throughout the experiment, the body weight of the mice was monitored as an indicator of cream toxicity.[93,94] Fig. 8(A) demonstrates that no significant weight loss was observed in any of the groups in the current study (p value > 0.05).

Following the induction of a solid tumor, the tumor volume was assessed in all groups, and all groups demonstrated significantly lower tumor volumes compared to the cancerous untreated group (p value < 0.05), as depicted in Fig. 8(B). The greatest inhibition of solid tumor progression was noticed in group VI treated with $P_{CG}5$ containing a higher ascorbyl glucoside concentration. The considerable tumor regression demonstrated in groups III and IV receiving the plain formulae ($P_{CG}1$ and $P_{CG}4$, respectively) highlights the anticancer effect of the enclosed ascorbyl glucoside in the proposed formulae.

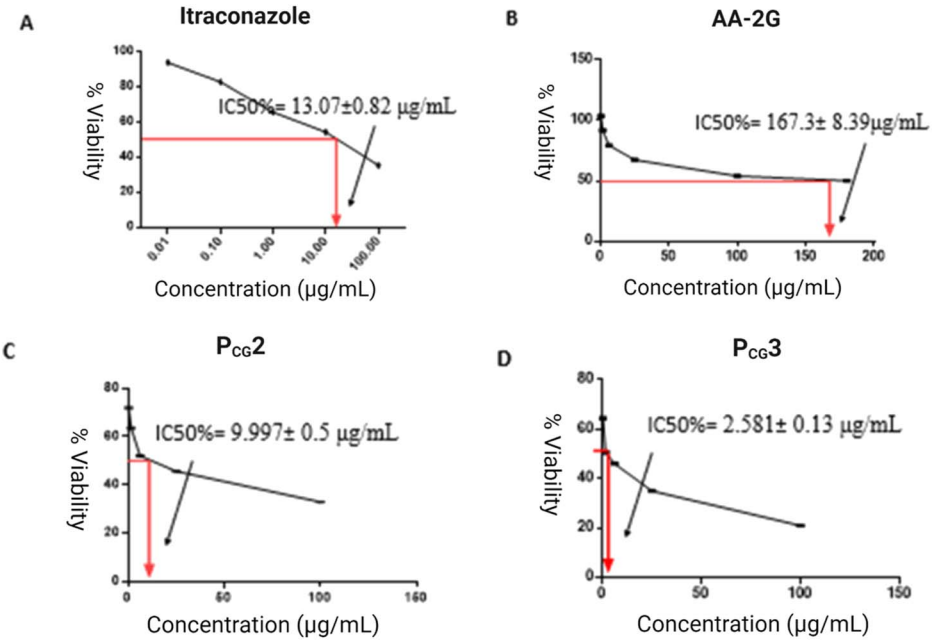

Fig. 6 Cytotoxicity of (A) itraconazole, (B) ascorbyl glucoside, (C) $P_{CG}2$ and (D) $P_{CG}3$ on A431 cells at 24 h using MTT assay. $P_{CG}2$: ITZ-glucospanlastics containing 10 mg AA-2G and 10 mg ITZ. $P_{CG}3$: ITZ-glucospanlastics containing 10 mg AA-2G and 20 mg ITZ.

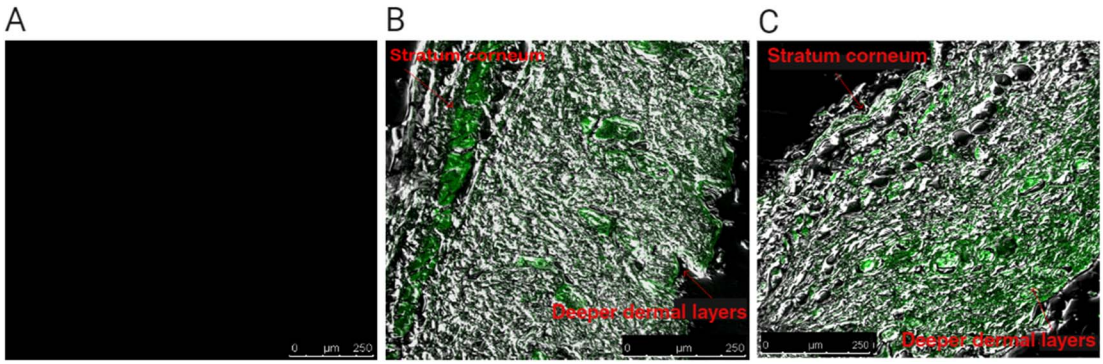

Fig. 7 CLSM images of a cross-section of abdominal mouse skin incubated on a Franz diffusion cell with Dil-loaded glucospanlastics by (10×) objective lens showing penetration and distribution of Dil fluorescent dye. (A) Control skin, (B) Dil-loaded glucospanlastics containing 10 mg ascorbyl glucoside $P_{CG}2$ and (C) Dil-loaded glucospanlastics containing 20 mg ascorbyl glucoside $P_{CG}5$. Scale bar (250 µm).

Following the completion of the study, the tumor weight was measured. Interestingly, the tumor weight followed the order of $P_{CG}5 < P_{CG}2 < P_{CG}4 < P_{CG}1 <$ conventional ITZ cream < cancerous untreated group, as illustrated in Fig. 8(C). These promising verifications motivated us to conduct histological analysis of the tumor tissues to visualize and quantify the extent of necrosis present in each treatment group as an indicator of tumor regression.

3.4.1. *In vivo* histopathological study. The histopathological examination conducted after the end of the study yielded noteworthy results, offering valuable insights into the confirmation of Ehrlich solid tumor progression and the potential therapeutic effects of the various treatments on the induced solid tumor. Fig. 9 displays the photomicrographs of the histological examinations conducted on the solid tumor tissues from the treated groups and the cancerous untreated group. In Fig. 9(A), group I (cancerous untreated control group) showed a subcutaneous wide thick zone of viable, pleomorphic and basophilic tumor cells (red star) with abundant mitotic figures (red arrows) and minimal central records of necrotic tissues (black star). The histopathological examination findings of the group treated with the conventional ITZ cream (group II), as shown in Fig. 9(B), depict minimal improvement with a mild increase in central necrotic mass (black star) compared with the model samples. Moreover, persistent higher records of thick viable tumor mass sheets were observed (red star) with many mitotic figures (red arrows).

Alternatively, the histopathological micrographs of the group treated with the plain glucospanlastics cream containing 10 mg of ascorbyl glucoside (group III, $P_{CG}1$), as shown in

Fig. 9(C), showed the same results as the conventional ITZ cream group. Interestingly, group IV treated with the plain glucospanlastic cream containing a higher concentration of ascorbyl glucoside (20 mg, $P_{CG}4$), as shown in Fig. 9(D), revealed moderate protective efficacy with persistent figures of viable tumor cells sheets (red star), moderate increase in central necrotic tissue debris (black star), many mitotic figures (red arrows) and moderate subcutaneous inflammatory cells infiltrates. These findings can be attributed to the significant role of ascorbyl glucoside, a hydrophilic derivative of vitamin C, in preventing skin oxidation and modulating the cellular signaling pathways involved in cell growth, differentiation, and cancer progression. Ascorbyl glucoside demonstrates the ability to reduce cancer cell viability and invasiveness, indicating its potential as a valuable component in skin cancer management.[95–97]

From skin health perspectives, crucially, ascorbic acid possess the following attributes: (i) formation of collagen in the dermis, (ii) photoprotection and prevention of skin oxidation (damage from ultraviolet radiation that is considered a risk factor for cutaneous malignancy development), (iii) modulation of pathways of cell growth and differentiation, and (iv) alleviation of inflammatory conditions.[29,95,96,98]

Optimally, the histopathological images of group V receiving $P_{CG}2$ formula (containing 20 mg AA2G and 10 mg ITZ), as shown in Fig. 9(E), showed a small-sized total tumor mass with a relatively significant higher necrotic tissue debris area percentage (black star) compared with the model group. Moreover, minimal mitotic tumor cells were observed among the peripheral viable tumor cells (red star).

Furthermore, the histopathological examination of group VI, as shown in Fig. 9(F), treated with formula $P_{CG}5$ showed almost the same results as group V together with a mild increase in necrotic tissue debris. This result is in good agreement with the evaluation of the tumor volume difference.

It is important to highlight that although the results regarding tumor volume did not provide sufficient evidence of efficacy, it is possible that specific regions within the tumor experienced cell death without a significant reduction in overall tumor volume. This occurrence is commonly observed as necrotic cell death within the core region of solid tumors.[99]

Interestingly, the percentage of necrosis increased with an increase in the amount of the incorporated AA2G. Both formulae ($P_{CG}2$ and $P_{CG}5$) containing the same amount of ITZ (10 mg) with different amounts of AA2G (10 and 20 mg, respectively) showed a considerable percentage of necrosis (48.4% ± 0.56%, and 57.85% ± 0.21%, respectively, as shown in Fig. 9(G)) with the relevant superiority of the latter containing a higher amount of AA2G ($P_{CG}5$, 20 mg). The presence of AA2G could potentiate the effect of ITZ, verifying its *in vitro* cytotoxic potential. Importantly, the nano size of ITZ-glucospanlastics could contribute to their improved permeation and localization within the target area, particularly when combined with the potent antioxidant properties of AA2G.[100]

Observing the necrosis index of the tested plain formulae further evidenced the competent anticancer effect of AA2G. Comparing the plain formulae ($P_{CG}1$ and $P_{CG}4$) containing two different amounts of AA2G (10 and 20 mg in group III and IV, respectively), it was found that there was a significant difference in the necrotic index (p value > 0.0001) between group III receiving the lowest amount of AA2G and group IV receiving the highest amount of AA2G, with the necrotic index of 40.45 ± 0.35% and 44.90 ± 1.27%, respectively as shown in Fig. 9(G). These values were almost 3-fold and 1.5-fold higher than that of the untreated group I (13.25 ± 0.63%) and conventional ITZ cream (28.25 ± 0.35%), respectively.

There was a remarkable difference observed in the tumor necrosis index for all the tested groups compared to the cancerous untreated group (p value < 0.0001). These findings are consistent with the results obtained from the reduction in tumor weight. The obtained results provide an explanation for the superiority of the plain glucospanlastic cream over the conventional ITZ cream, as evidenced by the reduction in tumor weight and the increase in tumor necrosis percentage. These findings underscore the significant role of the antioxidant AA-2G in promoting tumor cell death and improving the therapeutic outcomes.

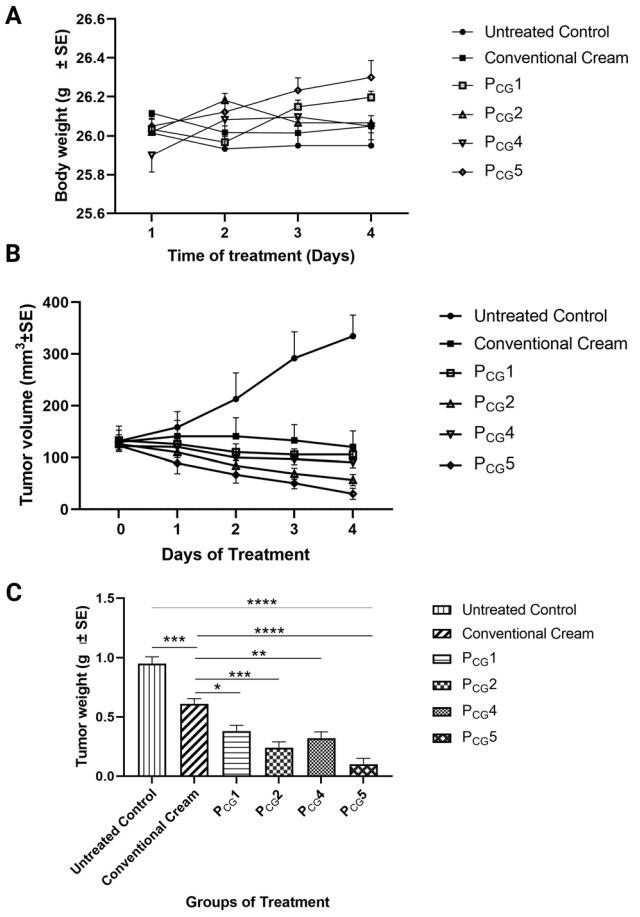

Fig. 8 (A) Body weight of all mouse groups in the EAC model, (B) tumor volume in all mouse groups, and (C) tumor weight after sacrifice. Values shown are mean ± SD ($n = 6$). *Significant at $p < 0.05$, and ***significant at $p < 0.001$ using one-way ANOVA followed by Tukey–Kramer post hoc test.

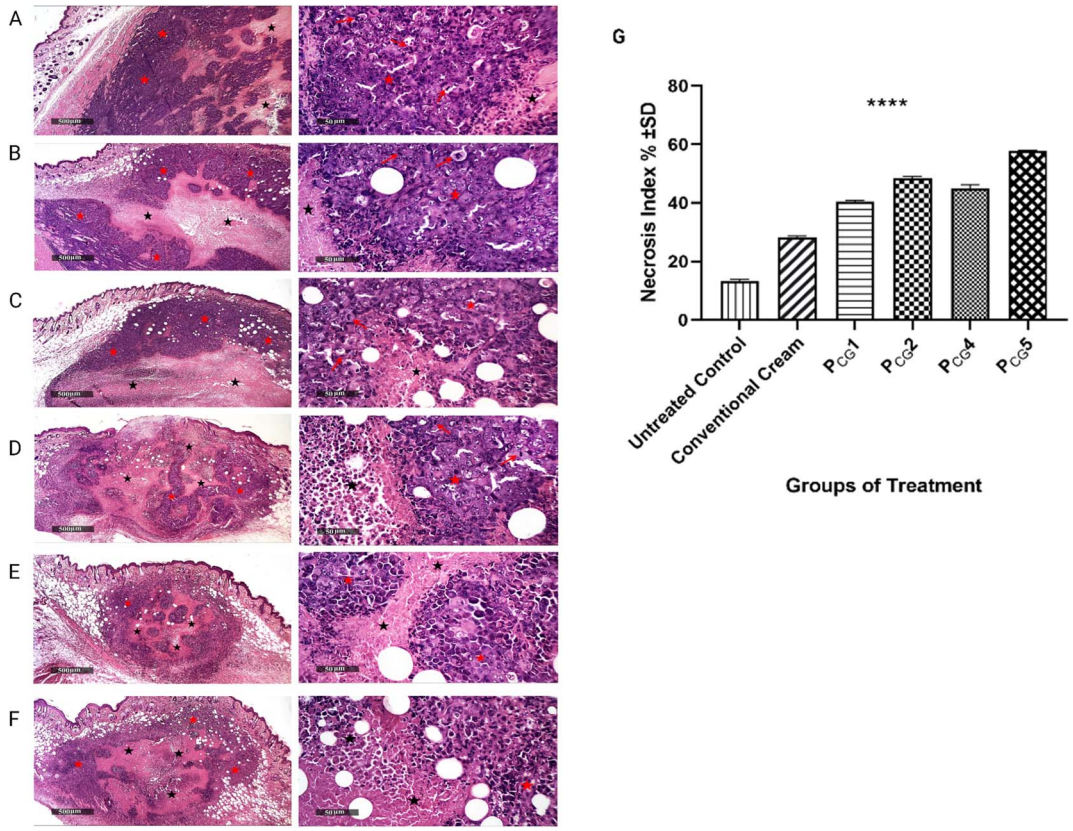

Fig. 9 Histopathological examination of tumor tissues of different animal groups at the end of *in vivo* study: untreated cancerous control (A), conventional ITZ cream (B), $P_{CG}1$ (C), $P_{CG}4$ (D), $P_{CG}2$ (E), $P_{CG}5$ and (F) (H&E stain) magnification power 40× and 400×. (G) % tumor necrosis for the processed histopathological samples of different animal groups. Results are expressed as mean ± SD, ($n = 6$) **significant at $p < 0.01$, ***significant at $p < 0.001$ and ****significant at $p < 0.0001$ using one-way ANOVA followed by Tukey–Kramer post hoc test.

3.4.2. Biochemical assessment of antioxidant markers in tumor mass. Essentially, the excessive accumulation of reactive oxygen species (ROS) surpassing the capacity of the natural antioxidant defense system leads to a condition known as oxidative stress. This oxidative stress is primarily responsible for chronic inflammation, which disrupts cellular function and promotes the proliferation of cancer cells.[101] According to the current theories of biomedicine, oxidative stress is one of the crucial pathophysiological processes involved in major stress- and age-associated diseases, including cancer. Consequently, antioxidants are usually thought to be a nearly universal defense that can avoid or even fight cancer. Glutathione (GSH) is the most abundant non enzymatic intracellular defense system, which is responsible for the elimination of damaging lipid peroxides and other ROS species. In this respect, the reduction in GSH (glutathione) content signifies the occurrence of cellular oxidation processes and lipid peroxidation.[102,103] The concentration of GSH was measured in the tumor homogenate and was found to be considerably heightened to variable degrees in all the treatment groups relative to the cancerous untreated group, as shown in Fig. 10(A). The drug-loaded glucospanlastic formulae ($P_{CG}2$ and $P_{CG}5$) yielded a significant improvement in GSH levels by 2.63- and 3.5-fold *vs.* the cancerous untreated group and 1.68- and 2.26-fold *vs.* the conventional ITZ cream, respectively (p value < 0.0001). Interestingly, the plain glucospanlastics $P_{CG}4$ and $P_{CG}1$ increased the content of GSH by 1.84- and 2.03-fold *vs.* the cancerous untreated group, respectively. Thus, the effect of the glucospanlastics formulated with a higher concentration of AA2G was more pronounced.

Malondialdehyde (MDA) is a prominent byproduct generated through the breakdown of peroxidized polyunsaturated fatty acids. Consequently, it serves as a commonly employed marker for assessing lipid peroxidation following damage caused by oxidative stress induced by free radicals. It is widely recognized that increased levels of MDA, observed in various pathological conditions including cancer, are closely associated with damage caused by free radicals. Conversely, a decrease in MDA levels can be expected following treatment with antioxidants, given that they mitigate oxidative stress and its detrimental effects. In our study, we detected a dramatic decrease in MDA content in response to the antioxidant effect induced by the $P_{CG}2$ and $P_{CG}5$ treatment groups (2.59- and 2.94-fold reduction *vs.* cancerous untreated group and 1.78- and 2.03-fold decrease *vs.* conventional ITZ cream group, respectively). This effect was also significantly attenuated by the incorporation of AA-2G given that the levels of MDA were significantly decreased in the plain glucospanlastic formulae ($P_{CG}4$ and $P_{CG}1$, p value < 0.001) in comparison to the conventional ITZ cream group, as shown in Fig. 10(B).

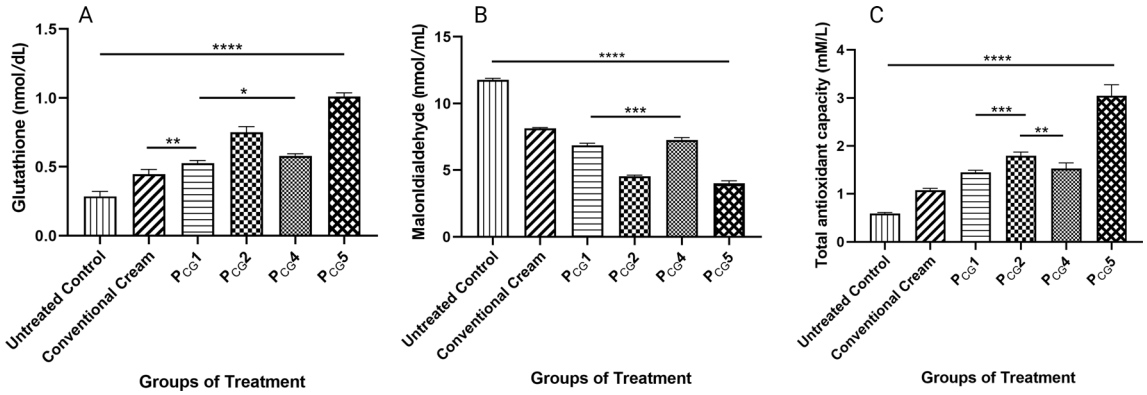

Fig. 10 The measurements of antioxidant parameters in tumor masses in EAC tumor-bearing mice at the end of *in vivo* study in the different groups of study, (A) glutathione, (B) malonldialdehyde, (C) total antioxidant capacity. Values shown are mean ± SD, ($n = 6$). *Significant at $p < 0.05$, **significant at $p < 0.01$, ***significant at $p < 0.001$ and ****significant at $p < 0.0001$ using one-way ANOVA followed by Tukey Kramer's post hoc test.

The total antioxidant capacity (TAC) is a measure of the overall antioxidant capacity in biological systems, including tissues and body fluids. It provides an assessment of the collective capacity of various antioxidants. The measurement of TAC considers the cumulative effect of different antioxidants, including enzymatic antioxidants (such as superoxide dismutase, catalase, and glutathione peroxidase) and non-enzymatic antioxidants (such as vitamins C and E, carotenoids, flavonoids, and polyphenols). TAC assays involve measuring the ability of a biological sample to scavenge or neutralize free radicals. According to the data presented in Fig. 10(C), notably all the treatment groups demonstrated significantly increased TAC values compared to the cancerous untreated group (p value < 0.0001), showing the same trend noticed with GSH. Groups V and VI receiving the drug-loaded glucospanlastic formulae ($P_{CG}2$ and $P_{CG}5$) displayed the highest TAC with values of 1.795 ± 0.077 and 3.045 ± 0.233 mM L^{-1} (3.01- and 5.51-fold increase *vs.* cancerous untreated group and 1.67- and 2.84-fold increase *vs.* conventional ITZ cream group), respectively. This indicates that the treatments had a positive impact on enhancing the overall antioxidant capacity in the tested groups.

The data suggest that the encapsulation of ITZ in the glucospanlastics with a higher concentration of AA2G provided better antioxidant activity together with an anticancer effect compared to the conventional ITZ cream and cancerous untreated groups.

4. Conclusion

In the present investigation, we designed and explored new vesicles by combining surfactant base vesicles, spanlastics (made of Span 60 and Tween 80), with AA-2G (glucospanlastics). The proposed vesicles showed nano-dimensions, noticeably affected by the AA-2G and Tween 80 ratio, negative surface charge, heightened solubilisation efficiency and ITZ entrapment coupled with antioxidant and cytotoxic effects. More specifically, they could permeate the deep skin strata. The formulated O/W cream enclosing the proposed glucospanlastics possessed the capability of suppressing an induced subcutaneous Ehrlich tumor, as reflected in the reduction in tumor size and weight and the boost in necrosis percentage and antioxidant levels. The newly developed glucospanlastics utilizing AA-2G as an ascorbic acid derivative represent antioxidant and anticancer nanovesicles, possessing the ability to maintain the features of AA, and also enhance the solubility of the hydrophobic ITZ. These promising attributes can yield nanoplatforms for anticancer topical therapy, which requires clinical verification.

Data availability

The authors confirm that the data supporting the findings of this study are available within the article and its ESI.†

Author contributions

Caroline Lamie, conceptualization, data curation, investigation, formal analysis, methodology, validation, and writing – original draft. Enas Elmowafy, conceptualization, data curation, investigation, formal analysis, methodology, validation, supervision, and writing – review & editing. Dalia Attia, conceptualization, data curation, formal analysis, supervision, and writing – review & editing. Nahed D. Mortada, conceptualization, formal analysis, data curation, supervision, and writing – review & editing.

Conflicts of interest

The authors declare no competing interests.

Acknowledgements

Associate professor Dr Mona Abdel Mottaleb for her help in confocal microscopy.

References

1 M. Tiboni, *et al.*, A combination of sugar esters and chitosan to promote in vivo wound care, *Int. J. Pharm.*, 2022, **616**, 121508.
2 D. K. Chandrasekharan, *et al.*, Synthesis of nanosilver using a vitamin C derivative and studies on radiation protection, *Cancer Biother.Radiopharm.*, 2011, **26**(2), 249–257.
3 A. C. Caritá, *et al.*, Vitamin C: One compound, several uses. Advances for delivery, efficiency and stability, *Nanomed. Nanotechnol. Biol. Med.*, 2020, **24**, 102117.
4 Y. Inoue, *et al.*, Application of ascorbic acid 2-glucoside as a solubilizing agent for clarithromycin: solubilization and nanoparticle formation, *Int. J. Pharm.*, 2007, **331**(1), 38–45.
5 S. Palma, *et al.*, Coagels from ascorbic acid derivatives, *Langmuir*, 2002, **18**(24), 9219–9224.
6 L. Li, *et al.*, Mechanism Study on Nanoparticle Negative Surface Charge Modification by Ascorbyl Palmitate and Its Improvement of Tumor Targeting Ability, *Molecules*, 2022, **27**(14), 4408.
7 C. Lamie, *et al.*, Diversifying the skin cancer-fighting worthwhile frontiers: How relevant are the itraconazole/ascorbyl palmitate nanovectors?, *Nanomed. Nanotechnol. Biol. Med.*, 2022, **43**, 102561.
8 W.-Y. Huang, *et al.*, Stability studies of ascorbic acid 2-glucoside in cosmetic lotion using surface response methodology, *Bioorg. Med. Chem. Lett.*, 2013, **23**(6), 1583–1587.
9 K. Miura and A. Tai, 2-O-α-D-Glucopyranosyl-l-ascorbic acid as an antitumor agent for infusion therapy, *Biochem. Biophys. Rep.*, 2017, **10**, 232–236.
10 K. Miura, *et al.*, Potential antitumor activity of 2-O-α-D-glucopyranosyl-6-O-(2-pentylheptanoyl)-L-ascorbic acid, *Int. J. Mol. Sci.*, 2018, **19**(2), 535.
11 C. Jacques, *et al.*, Ascorbic acid 2-glucoside: An ascorbic acid pro-drug with longer-term antioxidant efficacy in skin, *Int. J. Cosmet. Sci.*, 2021, **43**(6), 691–702.
12 C. H. Chen and W. Y. Gao, Ophthalmic product with antioxidative function, *US Pat. Appl.*, 16/896311, Pegavision Corp, 2020.
13 G. Nonaka and H. Tanaka, Skin care composition comprising skin lightening agent, *US Pat. Appl.*, 10/864693, Procter and Gamble Co, 2005.
14 K. M. R. Srivalli and B. Mishra, Improved aqueous solubility and antihypercholesterolemic activity of ezetimibe on formulating with hydroxypropyl-β-cyclodextrin and hydrophilic auxiliary substances, *AAPS PharmSciTech*, 2016, **17**(2), 272–283.
15 K. M. R. Srivalli and B. Mishra, Preparation and pharmacodynamic assessment of ezetimibe nanocrystals: Effect of P-gp inhibitory stabilizer on particle size and oral absorption, *Colloids Surf., B*, 2015, **135**, 756–764.
16 H. Onoda, *et al.*, Preparation and characterization of triamterene complex with ascorbic acid derivatives, *Drug Dev. Ind. Pharm.*, 2020, **46**(12), 2032–2040.
17 S. Kim, *et al.*, Physicochemical study of ascorbic acid 2-glucoside loaded hyaluronic acid dissolving microneedles irradiated by electron beam and gamma ray, *Carbohydr. Polym.*, 2018, **180**, 297–303.
18 S. Melo-Guímaro, *et al.*, Efficient dermal delivery of ascorbic acid 2-glucoside with photoacoustic waves, *Int. J. Cosmet. Sci.*, 2022, **44**(4), 453–463.
19 M. Jaber, *et al.*, Preparation and evaluation of ascorbyl glucoside and ascorbic acid solid in oil nanodispersions for corneal epithelial wound healing, *Int. J. Pharm.*, 2022, **627**, 122227.
20 S. Swaminathan, *et al.*, Formulation of betacyclodextrin based nanosponges of itraconazole, *J. Inclusion Phenom. Macrocyclic Chem.*, 2007, **57**(1), 89–94.
21 C. Carbone, *et al.*, Repurposing itraconazole to the benefit of skin cancer treatment: A combined azole-DDAB nanoencapsulation strategy, *Colloids Surf., B*, 2018, **167**, 337–344.
22 C. R. Chong, *et al.*, Inhibition of angiogenesis by the antifungal drug itraconazole, *ACS Chem. Biol.*, 2007, **2**(4), 263–270.
23 J. R. Pace, *et al.*, Formulation and evaluation of itraconazole liposomes for Hedgehog pathway inhibition, *J. Liposome Res.*, 2020, **30**(3), 305–311.
24 M. D. Ansari, *et al.*, Spanlastics a novel nanovesicular carrier: its potential application and emerging trends in therapeutic delivery, *AAPS PharmSciTech*, 2022, **23**(4), 112.
25 S. Rathod, *et al.*, Investigations on the role of edge activator upon structural transitions in Span vesicles, *Colloids Surf., A*, 2021, **627**, 127246.
26 E. Elmowafy, *et al.*, Novel antipsoriatic fluidized spanlastic nanovesicles: In vitro physicochemical characterization, ex vivo cutaneous retention and exploratory clinical therapeutic efficacy, *Int. J. Pharm.*, 2019, **568**, 118556.
27 M. Magdy, *et al.*, Glycerospanlastics: State-of-the-art two-in-one nano-vesicles for boosting ear drug delivery in otitis media treatment, *Int. J. Pharm.*, 2023, **645**, 123406.
28 J. D. Shultz, *et al.*, Design and development of raw clay-based formulations emulsions loaded with ascorbyl glucoside, in vitro evaluations on topical delivery and cell viability, *J. Dispersion Sci. Technol.*, 2024, **45**(4), 731–742.
29 A. Godic, *et al.*, The role of antioxidants in skin cancer prevention and treatment, *Oxid. Med. Cell. Longevity*, 2014, **2014**(1), 860479.
30 P. C. Capponi, D. Murri and C. Pernice, Topical L-ascorbic acid formulation for a better management of non-melanoma skin cancer: perspective for treatment strategies, *Pharmaceutics*, 2021, **13**(8), 1201.
31 G. Arumugam and S. Alagar Yadav, Synergistic inhibitory actions of resveratrol, epigallocatechin-3-gallate, and diallyl trisulfide against skin cancer cell line A431 through mitochondrial caspase dependent pathway: a combinational drug approach, *Med. Oncol.*, 2024, **41**(3), 64.
32 P. Laomethakorn, *et al.*, 13-Butoxyberberine Bromide Inhibits Migration and Invasion in Skin Cancer A431 Cells, *Molecules*, 2023, **28**(3), 991.

33 M. M. El Taweel, *et al.*, Tailoring of topically applied curcumin loaded pro-novasomes for skin cancer treatment: In-vitro characterization, statistical optimization and histopathological assessment of subcutaneous Ehrlich carcinoma mice model, *J. Drug Delivery Sci. Technol.*, 2023, **88**, 104957.
34 S. Kakkar and I. P. Kaur, Spanlastics—A novel nanovesicular carrier system for ocular delivery, *Int. J. Pharm.*, 2011, **413**(1–2), 202–210.
35 A. Y. Farrah, *et al.*, Investigating the potential of phosphatidylcholine-based nano-sized carriers in boosting the oto-topical delivery of caroverine: in vitro characterization, stability assessment and ex vivo transport studies, *Int. J. Nanomed.*, 2020, **15**, 8921.
36 K. A. Wadile, P. P. Ige and R. O. Sonawane, Preparation of itraconazole nanoparticles and its topical nanogel: Physicochemical properties and stability studies, *International Journal of Pharmaceutical Sciences and Developmental Research*, 2019, **5**(1), 001–008.
37 S. Franzè, *et al.*, Drug-in-micelles-in-liposomes (DiMiL) systems as a novel approach to prevent drug leakage from deformable liposomes, *Eur. J. Pharm. Sci.*, 2019, **130**, 27–35.
38 E. Elmowafy, *et al.*, Quercetin loaded monolaurate sugar esters-based niosomes: Sustained release and mutual antioxidant—hepatoprotective interplay, *Pharmaceutics*, 2020, **12**(2), 143.
39 E. Elmowafy, *et al.*, Exploring optimized methoxy poly (ethylene glycol)-block-poly (ε-caprolactone) crystalline cored micelles in anti-glaucoma pharmacotherapy, *Int. J. Pharm.*, 2019, **566**, 573–584.
40 İ. Gulcin and S. H. Alwasel, DPPH radical scavenging assay, *Processes*, 2023, **11**(8), 2248.
41 U. Shinde, S. Pokharkar and S. Modani, Design and evaluation of microemulsion gel system of nadifloxacin, *Indian J. Pharm. Sci.*, 2012, **74**(3), 237.
42 C. Lamie, *et al.*, Assessment of antifungal efficacy of itraconazole loaded aspasomal cream: comparative clinical study, *Drug Delivery*, 2022, **29**(1), 1345–1357.
43 A. S. Mohamed, S. R. Fahmy and A. A. Elsayed, Formulation and Evaluation of the sea cucumber, Holothuria arenicola extract incorporated skin cream, *GSC Biol. Pharm. Sci.*, 2020, **13**(2), 232–239.
44 R. Yehia, *et al.*, Anti-tumor efficacy of an integrated methyl dihydrojasmonate transdermal microemulsion system targeting breast cancer cells: in vitro and in vivo studies, *Colloids Surf., B*, 2017, **155**, 512–521.
45 S. Waz, *et al.*, Nephroprotective effect of exogenous hydrogen sulfide donor against cyclophosphamide-induced toxicity is mediated by Nrf2/HO-1/NF-κB signaling pathway, *Life Sci.*, 2021, **264**, 118630.
46 W. W. Ibrahim, *et al.*, Dapagliflozin as an autophagic enhancer via LKB1/AMPK/SIRT1 pathway in ovariectomized/d-galactose Alzheimer's rat model, *Inflammopharmacology*, 2022, **30**(6), 2505–2520.
47 D. Koracevic, *et al.*, Method for the measurement of antioxidant activity in human fluids, *J. Clin. Pathol.*, 2001, **54**(5), 356.
48 D. Aluani, *et al.*, Evaluation of biocompatibility and antioxidant efficiency of chitosan-alginate nanoparticles loaded with quercetin, *Int. J. Biol. Macromol.*, 2017, **103**, 771–782.
49 F. Badria and E. Mazyed, Formulation of Nanospanlastics as a Promising Approach for Improving the Topical Delivery of a Natural Leukotriene Inhibitor (3- Acetyl-11-Keto-β-Boswellic Acid): Statistical Optimization, in vitro Characterization, and ex vivo Permeation Study, *Drug Des., Dev. Ther.*, 2020, **14**, 3697.
50 M. D. Ansari, *et al.*, Spanlastics a Novel Nanovesicular Carrier: Its Potential Application and Emerging Trends in Therapeutic Delivery, *AAPS PharmSciTech*, 2022, **23**(4), 1–12.
51 A. Ahad, *et al.*, Formulation and characterization of Phospholipon 90 G and tween 80 based transfersomes for transdermal delivery of eprosartan mesylate, *Pharm. Dev. Technol.*, 2018, **23**(8), 787–793.
52 E. Alaaeldin, *et al.*, Spanlastics as an efficient delivery system for the enhancement of thymoquinone anticancer efficacy: Fabrication and cytotoxic studies against breast cancer cell lines, *J. Drug Delivery Sci. Technol.*, 2021, **65**, 102725.
53 G. M. El Zaafarany, *et al.*, Role of edge activators and surface charge in developing ultradeformable vesicles with enhanced skin delivery, *Int. J. Pharm.*, 2010, **397**(1–2), 164–172.
54 S. Silva, *et al.*, Evolution of the use of antioxidants in anti-ageing cosmetics, *Int. J. Cosmet. Sci.*, 2019, **41**(4), 378–386.
55 S. A. Tayel, *et al.*, Duodenum-triggered delivery of pravastatin sodium via enteric surface-coated nanovesicular spanlastic dispersions: development, characterization and pharmacokinetic assessments, *Int. J. Pharm.*, 2015, **483**(1–2), 77–88.
56 D. H. Khan, *et al.*, Process optimization of ecological probe sonication technique for production of rifampicin loaded niosomes, *J. Drug Delivery Sci. Technol.*, 2019, **50**, 27–33.
57 M. A. Elgewelly, *et al.*, Resveratrol-Loaded Vesicular Elastic Nanocarriers Gel in Imiquimod-Induced Psoriasis Treatment: In Vitro and In Vivo Evaluation, *J. Pharm. Sci.*, 2022, **111**(2), 417–431.
58 C. E. M. Dcruz, *et al.*, Novel nano spanlastic carrier system for buccal delivery of lacidipine, *J. Drug Delivery Sci. Technol.*, 2022, **68**, 103061.
59 S. Bhattacharjee, DLS and zeta potential–what they are and what they are not?, *J. Controlled Release*, 2016, **235**, 337–351.
60 V. Dave, *et al.*, Lipid-polymer hybrid nanoparticles: Development & statistical optimization of norfloxacin for topical drug delivery system, *Bioact. Mater.*, 2017, **2**(4), 269–280.
61 D. E. Aziz, A. A. Abdelbary and A. I. Elassasy, Investigating superiority of novel bilosomes over niosomes in the transdermal delivery of diacerein: in vitro characterization, ex vivo permeation and in vivo skin deposition study, *J. Liposome Res.*, 2019, **29**(1), 73–85.
62 M. A. Abdelbari, *et al.*, Implementing spanlastics for improving the ocular delivery of clotrimazole: in vitro

characterization, ex vivo permeability, microbiological assessment and in vivo safety study, *Int. J. Nanomed.*, 2021, **16**, 6249.

63 A. N. ElMeshad and A. M. Mohsen, Enhanced corneal permeation and antimycotic activity of itraconazole against Candida albicans via a novel nanosystem vesicle, *Drug Delivery*, 2016, **23**(7), 2115–2123.

64 A. Saleh, *et al.*, Zolmitriptan intranasal spanlastics for enhanced migraine treatment; formulation parameters optimized via quality by design approach, *Sci. Pharm.*, 2021, **89**(2), 24.

65 A. H. Alomrani, *et al.*, Itraconazole-hydroxypropyl-β-cyclodextrin loaded deformable liposomes: in vitro skin penetration studies and antifungal efficacy using Candida albicans as model, *Colloids Surf., B*, 2014, **121**, 74–81.

66 X. Ling, *et al.*, Development of an itraconazole encapsulated polymeric nanoparticle platform for effective antifungal therapy, *J. Mater. Chem. B*, 2016, **4**(10), 1787–1796.

67 L. De Smet, *et al.*, Formulation of itraconazole nanococrystals and evaluation of their bioavailability in dogs, *Eur. J. Pharm. Biopharm.*, 2014, **87**(1), 107–113.

68 R. H. Müller, C. Jacobs and O. Kayser, Nanosuspensions as particulate drug formulations in therapy: rationale for development and what we can expect for the future, *Adv. Drug Delivery Rev.*, 2001, **47**(1), 3–19.

69 Y. Inoue, *et al.*, Application of ascorbic acid 2-glucoside as a solubilizing agent for clarithromycin: solubilization and nanoparticle formation, *Int. J. Pharm.*, 2007, **331**(1), 38–45.

70 M. Manconi, *et al.*, Penetration enhancer-containing vesicles: composition dependence of structural features and skin penetration ability, *Eur. J. Pharm. Biopharm.*, 2012, **82**(2), 352–359.

71 P. Eaton, *et al.*, A direct comparison of experimental methods to measure dimensions of synthetic nanoparticles, *Ultramicroscopy*, 2017, **182**, 179–190.

72 N. A. El-Sheridy, *et al.*, Itraconazole lipid nanocapsules gel for dermatological applications: in vitro characteristics and treatment of induced cutaneous candidiasis, *Colloids Surf., B*, 2019, **181**, 623–631.

73 H. Kim, *et al.*, Characteristics of skin deposition of itraconazole solubilized in cream formulation, *Pharmaceutics*, 2019, **11**(4), 195.

74 H. P. Thakkar, *et al.*, Formulation and evaluation of liquisolid compacts of itraconazole to enhance its oral bioavailability, *Ther. Delivery*, 2020, **11**(2), 83–96.

75 B. Jaleh and P. Fakhri, Infrared and Fourier transform infrared spectroscopy for nanofillers and their nanocomposites, in *Spectroscopy of Polymer Nanocomposites*, Elsevier, 2016, pp. 112–129.

76 M. Khalil, *et al.*, Chitosan coated liposomes (CCL) containing triamcinolone acetonide for sustained delivery: A potential topical treatment for posterior segment diseases, *Int. J. Biol. Macromol.*, 2020, **143**, 483–491.

77 J. Fadke, J. Desai and H. Thakkar, Formulation development of spherical crystal agglomerates of itraconazole for preparation of directly compressible tablets with enhanced bioavailability, *AAPS PharmSciTech*, 2015, **16**(6), 1434–1444.

78 W. Yang, *et al.*, In vitro characterization and pharmacokinetics in mice following pulmonary delivery of itraconazole as cyclodextrin solubilized solution, *Eur. J. Pharm. Sci.*, 2010, **39**(5), 336–347.

79 S. Ismail and A. Khattab, Optimization of proniosomal itraconazole formulation using Box Behken design to enhance oral bioavailability, *J. Drug Delivery Sci. Technol.*, 2018, **45**, 142–150.

80 A. Farmoudeh, *et al.*, Methylene blue-loaded niosome: preparation, physicochemical characterization, and in vivo wound healing assessment, *Drug Delivery Transl. Res.*, 2020, **10**(5), 1428–1441.

81 Y. Inoue, *et al.*, Application of ascorbic acid 2-glucoside as a solubilizing agent for clarithromycin: solubilization and nanoparticle formation, *Int. J. Pharm.*, 2007, **331**(1), 38–45.

82 M. M. El-Sayed, *et al.*, Flurbiprofen-loaded niosomes-in-gel system improves the ocular bioavailability of flurbiprofen in the aqueous humor, *Drug Dev. Ind. Pharm.*, 2017, **43**(6), 902–910.

83 D. Fathalla, E. M. K. Youssef and G. M. Soliman, Liposomal and ethosomal gels for the topical delivery of anthralin: preparation, comparative evaluation and clinical assessment in psoriatic patients, *Pharmaceutics*, 2020, **12**(5), 446.

84 Y. Fujinami, A. Tai and I. Yamamoto, Radical scavenging activity against 1, 1-diphenyl-2-picrylhydrazyl of ascorbic acid 2-glucoside (AA-2G) and 6-acyl-AA-2G, *Chem. Pharm. Bull.*, 2001, **49**(5), 642–644.

85 J. Takebayashi, *et al.*, Antioxidant properties of 2-O-β-D-glucopyranosyl-L-ascorbic acid, *Biosci., Biotechnol., Biochem.*, 2008, **72**(6), 1558–1563.

86 R. Karim, *et al.*, Enhanced and preferential internalization of lipid nanocapsules into human glioblastoma cells: effect of a surface-functionalizing NFL peptide, *Nanoscale*, 2018, **10**(28), 13485–13501.

87 G. Lollo, *et al.*, Drug delivery to tumours using a novel 5-FU derivative encapsulated into lipid nanocapsules, *J. Drug Targeting*, 2019, **27**(5–6), 634–645.

88 P. Wiji Prasetyaningrum, A. Bahtiar and H. Hayun, Synthesis and cytotoxicity evaluation of novel asymmetrical mono-carbonyl analogs of curcumin (AMACs) against Vero, HeLa, and MCF7 Cell Lines, *Sci. Pharm.*, 2018, **86**(2), 25.

89 M. M. A. Abdel-Mottaleb, *et al.*, Stability of fluorescent labels in PLGA polymeric nanoparticles: Quantum dots versus organic dyes, *Int. J. Pharm.*, 2015, **494**(1), 471–478.

90 M. Lukić, I. Pantelić and S. D. Savić, Towards optimal ph of the skin and topical formulations: From the current state of the art to tailored products, *Cosmetics*, 2021, **8**(3), 69.

91 K. A. U. S. H. I. T. A. Banerjee, N. Thiagarajan and P. Thiagarajan, Formulation Optimization, Rheological Characterization and Suitability Studies of Polyglucoside-based Azadirachta indica A. Juss Emollient Cream as a Dermal Base for Sun Protection Application, *Indian J. Pharm. Sci.*, 2017, **79**(6), 914–922.

92 N. K. B. El-Din, D. A. Ali and R. F. Abou-El-Magd, Grape seeds and skin induce tumor growth inhibition via G1-phase arrest and apoptosis in mice inoculated with Ehrlich ascites carcinoma, *Nutrition*, 2019, **58**, 100–109.
93 S. C. Kim, *et al.*, In vivo evaluation of polymeric micellar paclitaxel formulation: toxicity and efficacy, *J. Controlled Release*, 2001, **72**(1–3), 191–202.
94 S. O. Ogbonnia, *et al.*, Antimicrobial evaluation, acute and subchronic toxicity studies of Leone Bitters, a Nigerian polyherbal formulation, in rodents, *Agric. Biol. J. North Am.*, 2010, **1**(3), 366–376.
95 M. Ponec, *et al.*, The formation of competent barrier lipids in reconstructed human epidermis requires the presence of vitamin C, *J. Invest. Dermatol.*, 1997, **109**(3), 348–355.
96 S. Ohno, *et al.*, High-dose vitamin C (ascorbic acid) therapy in the treatment of patients with advanced cancer, *Anticancer Res.*, 2009, **29**(3), 809–815.
97 K.-A. Lee, *et al.*, Hesperidin induces apoptosis by inhibiting Sp1 and its regulatory protein in MSTO-211H cells, *Biomol. Ther.*, 2012, **20**(3), 273.
98 M. Y. Lee and S. K. Chung, Treatment of corneal neovascularization by topical application of ascorbic acid in the rabbit model, *Cornea*, 2012, **31**(10), 1165–1169.
99 S. Y. Lee, M. K. Ju, H. M. Jeon, E. K. Jeong, Y. J. Lee, C. H. Kim, *et al.*, Regulation of tumor progression by programmed necrosis, *Oxid. Med. Cell. Longevity*, 2018, **2018**(1), 3537471.
100 R. M. Khalil, *et al.*, Development of lecithin/chitosan nanoparticles for promoting topical delivery of propranolol hydrochloride: Design, optimization and in-vivo evaluation, *J. Pharm. Sci.*, 2021, **110**(3), 1337–1348.
101 J. Kruk and E. Duchnik, Oxidative stress and skin diseases: possible role of physical activity, *Asian Pac. J. Cancer Prev.*, 2014, **15**(2), 561–568.
102 S. Raj Rai, *et al.*, Glutathione: role in oxidative/nitrosative stress, antioxidant defense, and treatments, *ChemistrySelect*, 2021, **6**(18), 4566–4590.
103 R. Masella, *et al.*, Novel mechanisms of natural antioxidant compounds in biological systems: involvement of glutathione and glutathione-related enzymes, *J. Nutr. Biochem.*, 2005, **16**(10), 577–586.